JOURNAL OF PETROLOGY | VOLUME 36 | NUMBER 6 | PAGES 1607–1631 | 1995

JACQUELINE EABY DIXON[1]*, EDWARD M. STOLPER[2] AND JOHN R. HOLLOWAY[2]
[1]DIVISION OF GEOLOGICAL AND PLANETARY SCIENCES, CALIFORNIA INSTITUTE OF TECHNOLOGY, PASADENA, CA 91125, USA
[2]DEPARTMENTS OF CHEMISTRY AND GEOLOGY, ARIZONA STATE UNIVERSITY, TEMPE, AZ 85287, USA

An Experimental Study of Water and Carbon Dioxide Solubilities in Mid-Ocean Ridge Basaltic Liquids. Part I: Calibration and Solubility Models

Experiments were conducted to determine the solubilities of H_2O and CO_2 and the nature of their mixing behavior in basaltic liquid at pressures and temperature relevant to seafloor eruption. Mid-ocean ridge basaltic (MORB) liquid was equilibrated at 1200°C with pure H_2O at pressures of 176–717 bar and H_2O–CO_2 vapor at pressures up to 980 bar. Concentrations and speciation of H_2O and CO_2 dissolved in the quenched glasses were measured using IR spectroscopy. Molar absorptivities for the 4500 cm^{-1} band of hydroxyl groups and the 5200 and 1630 cm^{-1} bands of molecular water are $0{\cdot}67 \pm 0{\cdot}03$, $0{\cdot}62 \pm 0{\cdot}07$, and 25 ± 3 l/mol-cm, respectively. These and previously determined molar absorptivities for a range of silicate melt compositions correlate positively and linearly with the concentration of tetrahedral cations (Si + Al).

*The speciation of water in glass quenched from vapor–saturated basaltic melt is similar to that determined by Silver & Stolper (*Journal of Petrology ***30****, 667–709, 1989) in albitic glass and can be fitted by their regular ternary solution model using the coefficients for albitic glasses. Concentrations of molecular water measured in the quenched basaltic glasses are proportional to f_{H_2O} in all samples regardless of the composition of the vapor, demonstrating that the activity of molecular water in basaltic melts follows Henry's law at these pressures. A best fit to our data and existing higher-pressure water solubility data (Khitarov* et al., Geochemistry ***5****, 479–492, 1959; Hamilton* et al., Journal of Petrology ***5****, 21–39, 1964), assuming Henrian behavior for molecular water and that the dependence of molecular water content on total water content can be described by the regular solution model, gives estimates for the $V^{o,m}_{H_2O}$ of 12 ± 1 cm^3/mol and for the 1-bar water solubility of $0{\cdot}11$ wt %.*

Concentrations of CO_2 dissolved as carbonate in the melt for pure CO_2-saturated and mixed H_2O–CO_2-saturated experiments are a simple function of f_{CO_2}. These results suggest Henrian behavior for the activity of carbonate in basaltic melt and do not support the widely held view that water significantly enhances the solution of carbon dioxide in basaltic melts. Using a $\Delta V_r^{o,m}$ of 23 cm^3/mol (Pan et al., Geochimica et Cosmochimica Acta ***55****, 1587–1595, 1991), the solubility of carbonate in the melt at 1 bar and 1200°C is 0·5 p.p.m. Our revised determination of CO_2 solubility is ~20% higher than that reported by Stolper & Holloway (*Earth and Planetary Science Letters ***87****, 397–408, 1988).*

KEY WORDS: *mid-ocean ridge basalts; water and carbon dioxide solubility; experimental petrology*

INTRODUCTION

Subaerial magmas solidify at a pressure of ~1 bar, but the pressure on submarine magmas ranges from near 1 bar to several hundred bars, depending on the water depth at which they erupt. Even over this small pressure range, the vesicularity and vesicle-gas composition of submarine magmas of constant bulk composition can change dramatically, reflecting the large differences in volume between gaseous and melt species, the large compressibility of the gas phase at these low pressures, and the increasing (but different) solubilities of all gaseous species with pressure in this pressure range. Thus, the well-known negative correlation between eruption depth and vesicularity of submarine magmas reflects the degassing of magmas at progressively lower pressures under conditions where the exsolving vapor is unable to escape fully from the magma (e.g. Moore, 1965,

*Corresponding author. Present address: Rosenstiel School of Marine and Atmospheric Science, Division of Marine Geology and Geophysics, University of Miami, Miami, FL 33149-1098, USA

1970, 1979; Moore & Schilling, 1973). Likewise, the different solubilities of the major (e.g. CO_2, H_2O, S) and minor (e.g. rare gases) volatile species are expected (though not yet observed) to lead to a strong dependence of the composition of the vapor in the vesicles on depth (e.g. Moore, 1965, 1970; Jambon *et al.*, 1985; Gerlach, 1986; Jambon *et al.*, 1986; Zhang & Zindler, 1989; Bottinga & Javoy, 1990*b*). Similarly, it is thought that differing solubilities of oxidized and reduced gaseous species can result in systematic changes in the oxidation state of iron and sulfur in erupting magmas as a function of the degree and depth of degassing (e.g. Sato, 1978; Mathez, 1984; Carmichael & Ghiorso, 1986; Christie *et al.*, 1986; Wallace & Carmichael, 1992; Nilsson & Peach, 1993).

In view of the importance of the exsolution of a vapor phase from submarine magmas in understanding their vesicle contents, their eruptive style, aspects of their chemistry, and ultimately the chemistry of the atmosphere and ocean (e.g. Javoy *et al.*, 1982; Des Marais, 1985; Marty & Jambon, 1987; Gerlach, 1989; Zhang & Zindler, 1989, 1993), it is surprising how little is known about the behavior of volatile components in these systems in the pressure range over which these magmas are erupted. For example, only recently has the solubility of carbon dioxide, the major component of vesicle gases in mid-ocean ridge basalt (MORB) (Killingley & Muenow, 1975; Moore *et al.*, 1977; Delaney *et al.*, 1978; Jambon & Zimmermann, 1987), been measured in MORB melt by experiment (Stolper & Holloway, 1988; Shilobreyeva & Kadik, 1989; Mattey, 1991; Pan *et al.*, 1991; Pawley *et al.*, 1992; Trull *et al.*, 1992). Water is even more abundant than carbon dioxide in most MORB glasses, but we know of no measurements of the solubility of water in MORB liquids at eruptive conditions, although water solubilities have been measured at higher pressures (1–10 kbar) in other basaltic compositions (Khitarov *et al.*, 1959; Hamilton *et al.*, 1964; Kadik *et al.*, 1971). Kadik *et al.* (1972) reported mixed CO_2 and H_2O solubilities in basaltic melts at 1–3 kbar, but their experiments did not extend to the CO_2-rich part of the system most relevant to MORBs, and their reported CO_2 solubility is inconsistent with more recent studies (Stolper & Holloway, 1988; Mattey, 1991; Pan *et al.*, 1991; Pawley *et al.*, 1992; Trull *et al.*, 1992).

In the context of MORB petrogenesis, the concentrations of water or carbon dioxide in basaltic liquids in equilibrium with pure water or carbon dioxide vapor are less important than their concentrations in liquids in equilibrium with H_2O–CO_2 fluids [as measured, for example, in the experiments of Kadik *et al.* (1972)], because the vapor that exsolves from MORB on decompression contains both volatile components. If both water and carbon dioxide activities in the mixed volatile system could be approximated by Henry's law (where the concentration of a species or component dissolved in the melt is proportional to its activity in the vapor) under the conditions of MORB genesis, then the behavior of the mixed volatile system could be understood simply with reference to the two end-member systems. Models of the degassing of magmas as they decompress based on the Henrian approximation and knowledge of the solubilities of CO_2 and H_2O in melts in the end-member systems have been presented by Shilobreyeva *et al.* (1983), Gerlach (1986), Newman (1989, 1990) and Bottinga & Javoy (1990*b*) for basaltic systems, and by Newman *et al.* (1988) for rhyolitic systems. However, data at higher pressures (i.e. greater than a few kilobars) in several silicate–H_2O–CO_2 systems including tholeiitic basalt have indicated that water enhances the amount of carbon dioxide that dissolves in vapor-saturated melt by as much as 50% (Eggler, 1973; Holloway & Lewis, 1974; Kadik & Eggler, 1975; Mysen *et al.*, 1975, 1976; Brey & Green, 1976; Mysen, 1976; Eggler & Rosenhauer, 1978; Holloway, 1981). In contrast, in their study of basaltic melts at 1–3 kbar, Kadik *et al.* (1972) did not find the effect of water on CO_2 concentration that would have been expected based on the later experiments at higher pressures. Also, recent low-pressure work on rhyolitic melts, in which carbon dioxide dissolves nearly entirely as CO_2 molecules, shows Henry's law describes well the behavior of carbon dioxide under these conditions (Blank *et al.*, 1993*a*). Thus, there is no consensus on the effect of water on the concentration of carbon dioxide (or vice versa) in vapor-saturated basaltic melts at pressures relevant to submarine eruption, despite its critical importance for interpreting measured volatile contents of submarine magmas and modeling their degassing behavior.

In this paper we report measurements of the solubility of water in MORB liquids at 1200°C at pressures under 1 kbar and of the mutual effects of water and carbon dioxide on each other's concentrations in vapor-saturated melts under these conditions. Concentrations of molecular water, hydroxyl groups and carbonate ion complexes in quenched glasses from the vapor-saturated experiments were measured by IR spectroscopy and used as a basis for developing a simple thermodynamic treatment of mixed-volatile solubility in MORB melts. Application of the results to modeling equilibrium degassing of ascending MORB magmas, interpreting the water and carbon contents of submarine magmas, and assessing the

factors controlling degassing of magmas during ascent and emplacement are presented in a separate paper (Part II, Dixon & Stolper, 1995).

EXPERIMENTAL TECHNIQUES

Experiments were conducted by equilibrating basaltic melt with pure H_2O, pure CO_2 and mixed H_2O–CO_2 vapors at 1200°C at pressures between 200 and 980 bar in conventional and rapid-quench internally heated pressure vessels. After quenching, the water and carbon dioxide contents of the basaltic glass were measured using IR spectroscopy. Vapor-phase compositions of some runs were determined by manometry. Experimental conditions and results for each experiment are given in Table 1.

Starting materials and capsules

Experiments were conducted on two starting materials, both Fe-rich basaltic glasses from the Juan de Fuca Ridge, chosen for their low liquidus temperatures of ~1165°C at 1 atm (Stolper & Holloway, 1988). Both glasses are nearly aphyric and have <1% vesicles. Compositions of the starting materials are listed in Table 2. Pretreatment of the starting materials is described in the footnote to Table 1. Powdered basalt (50–100 mg) and various combinations of water, oxalic acid dihydrate ($H_2C_2O_4 \cdot 2H_2O$) or silver oxalate ($Ag_2C_2O_4$) were loaded into Pt capsules (0·15-in. outside diameter tubing). The double-capsule technique (Van der Laan & Koster van Groos, 1991) was used in two-thirds of the experiments to minimize Fe loss to the Pt capsule. The remaining third of the experiments were performed using pure capsules. Capsules were sealed by arc welding and loaded into internally heated pressure vessels.

Conventional internally heated pressure vessel (IHPV)

Several low-pressure (200–300 bar) experiments in which basaltic melt and water were equilibrated were conducted in a horizontal, internally heated gas-pressure vessel (Holloway, 1971). Ar–H_2 gas mixtures were used as the pressurizing medium; total pressure was monitored with a Bourdon tube gauge. Hydrogen pressures in the Ar–H_2 gas, monitored using a AgPd Shaw membrane, were chosen so as to be approximately in equilibrium with H_2O at the quartz–fayalite–magnetite buffer (QFM) at the run conditions (Table 1). Samples were placed in the hot spot of a single-wound Kanthal furnace. Two sheathed chromel–alumel thermocouples bracketed the position of the capsule; one was used as input to an electronic temperature controller and the second was used to monitor temperature independently. Temperature gradients based on these two thermocouples were ~30°C along the length of the capsule. Single-pressure runs were held at the run conditions for 2·5 h. Reversals were held at a higher pressure for 2·5 h, and then the pressure was decreased and held at the final value for an additional 2·5 h. Pressures varied by <1% once the final pressure was reached in an experiment. Runs were terminated by shutting off power to the furnace, resulting in quench rates of ~8°C/s. Glasses were produced on quenching of H_2O-saturated experiments done in this apparatus at total pressures ≤300 bar. Melts from H_2O-saturated experiments conducted in this apparatus at higher pressures quenched to crystalline aggregates with minor amounts of glass.

Rapid-quench internally heated pressure vessel

Because of the difficulty in quenching water-saturated basaltic melts to glass at all but the lowest pressures (corresponding to total dissolved water contents less than ~1·8 wt %) in the conventional internally heated pressure vessels, a rapid-quench mechanism for the internally heated pressure vessel was designed for the higher-pressure experiments. Details of the design have been given by Holloway *et al.* (1992) and are summarized below. The pressure vessel was mounted in a vertical position. Samples were hung from a 0·2 mm diameter Pt wire in a double-wound Kanthal furnace. Four sheathed chromel–alumel thermocouples or three Pt–Rh (Pt/Pt–13Rh) thermocouples were spaced along the length of the capsule (~1·5 cm); one was used as input to an electronic temperature controller and the others were used to monitor temperature. Temperature gradients based on these thermocouples were typically <10°C over the length of the sample. Although several runs were conducted using pure Ar gas as the pressurizing medium, most were done using premixed Ar–H_2 gas (Table 1); pressures were monitored with a Bourdon tube gauge. The inclusion of quench wire leads through the head left insufficient room for a Shaw membrane, so P_{H_2} (i.e. the partial pressure of hydrogen) was assumed to be fixed in each experiment by the initial concentration of H_2 in the Ar–H_2 gas (Table 1). The validity of this assumption and its implications for f_{O_2} control are considered in the Results and Discussion ('Major element composition, Fe loss and oxidation state'). Experiments were either brought directly to the run conditions or first preequilibrated at a higher initial pressure as described above for the conventional IHPV experiments. The quenching mechanism used

Table 1: Summary of experimental results conducted at 1200°C

Experiment no.	7	8	9	17H	17M	18M	20H	20M	21H	21M	32A	33A	33B	34B	35B
Run conditions															
Starting material	a	a	a	a	a	a	a	a	b	b	c	c	c	c	c
P (bars)	206	201	300	717	717	980	310	310	507	507	515	503	503	507	504
Duration (h)	2·5	5	4·5	3	3	3	6	6	5·5	5·5	2	2	2	2	2
Reversal	no	yes	yes	no	no	no	yes	yes	yes	yes	no	no	no	no	no
Fe loss control	d	d	d	d	d	d	d	d	d	d	e	e	e	e	e
Init. Fe in Pt foil[f]	7·7	8·2	6·9	9·2	9·4	7·7	8·6	8·6	6·0	8·1					
Fe in Pt foil[g]				9·2±0·4			7·9±0·7		6·2±0·6	8·2±0·2					
log f_{O_2}[h]	−7·1	−7·2	−6·8	−7·7	−7·7	−7·0	−7·1	−7·7	−6·5	−7·2					
ΔQFM[i]	+1·4	+1·2	+1·6	+0·7	+0·7	+1·5	+1·3	+0·8	+2·0	+1·3					
X_{H_2} in Ar–H_2 gas	0·0195[j]	0·0210[j]	0·0193[j]	0·0149[k]	0·0149[k]	0·0149[k]	0·0149[k]	0·0149[k]	0·0149[k]	0·0149[k]	0[l]	0[l]	0[l]	0[l]	0[l]
log f_{O_2}[m]	−8·4	−8·5	−8·5	−8·3	−11·6	−9·2	−8·2	−9·1	−8·3	−9·1					
ΔQFM[i]	+0·0	−0·0	+0·0	+0·2	−3·1	−0·7	+0·2	−0·6	+0·2	−0·6					
Rapid quench	no	no	no	yes	yes	yes	yes	yes	yes	yes	yes	yes	yes	yes	yes
Glass															
FeO*[n]	12·0	12·0	12·0	13·1	12·1	11·5	11·9	11·9	11·4	11·9	10·1	10·4	10·3	9·88	n.a.
FeO[o]	9·57	9·71	8·72	9·41	10·02	9·79	9·47	6·56	9·11	10·0	n.a.	4·15	1·95	0·48	n.a.
Fe_2O_3[p]	2·70	2·54	3·69	4·06	2·34	1·86	2·64	5·98	2·53	2·09	n.a.	6·79	9·23	10·44	n.a.
log f_{O_2}[q]	−7·4	−7·5	−6·6	−6·7	−7·9	−8·1	−7·4	−5·0	−7·4	−7·9		−5·9	−1·8	1·2	
ΔQFM[i]	+1·1	+1·0	+1·9	+1·8	+0·6	+0·4	+1·1	+3·5	+1·1	+0·5		+2·6	+6·7	+9·7	
ρ (g/cm^3)[r]	2·87	2·86	2·86	2·86	2·88	2·83	2·84	2·86	2·83	2·85	2·84	2·84	2·84	2·84	2·88

JOURNAL OF PETROLOGY VOLUME 36 NUMBER 6 DECEMBER 1995

Vapor															
H_2O loaded (μmol)	150	234	212	570	0	281	333	97	487	163	48	71	170	161	52
CO_2 loaded (μmol)	0	0	0	0	274	281	0	97	0	163	185	134	57	34	119
Final H_2O (μmol)															
mass balance[s]	85(2)	162(9)	124(6)	431(8)		186(2)	265(1)	56(2)	377(2)	108(0)	29(2)	50(2)	121(1)	114(3)	37(1)
manometry[t]	n.a.	n.a.	n.a.	n.a.	n.a.	n.a.	n.a.	60	n.a.	110	n.a.	n.a.	n.a.	n.a.	n.a.
H_2O, mol[u]					8			61		134	28	39	79	76	4
Final CO_2 (μmol)															
mass balance[s]	0	0	0	0	273	280	0	97	0	163	185	133	57	34	119
manometry[t]	n.a.	n.a.	n.a.	n.a.	n.a.	n.a.	n.a.	96	n.a.	161	n.a.	n.a.	n.a.	n.a.	n.a.
H_2O, mol[u]								97		163	185	133	57	34	119
Dissolved volatiles															
wt basalt powder (g)	0·09166	0·09059	0·09071	0·10135	0·10086	0·09218	0·07125	0·07090	0·08900	0·09282	0·04186	0·04435	0·05330	0·052970	0·07212
Initial H_2O in basalt (wt%)	0	0	0	0	0	0	0	0	0·36	0·36	0	0	0	0	0
Total water (wt%)[v]	1·28(0·03)	1·43(0·18)	1·74(0·12)	2·49(0·15)	0·48(0·02)	1·83(0·03)	1·71(0·02)	1·02(0·04)	2·23(0·05)	1·41(0·00)	0·83(0·07)	0·86(0·06)	1·67(0·04)	1·58(0·10)	0·37(0·02)
(μmol)	65(2)	72(9)	88(6)	140(8)	27(1)	95(2)	68(1)	41(2)	110(2)	74(0)	19(2)	21(2)	49(1)	47(3)	15(1)
OH (wt%)[w]	0·91(·02)	0·97(0·04)	1·16(0·03)	1·64(0·15)	0·37(0·03)	1·43(0·18)	1·13(0·02)	0·89(0·02)	1·34(0·06)	1·06(0·05)	0·73(0·06)	0·71(0·04)	1·25	1·28(0·03)	0·47(0·06)
Molecular H_2O (wt%)[x]	0·27(0·01)	0·36(0·04)	0·53(0·02)	0·90(0·07)	0·02(0·00)	0·51(0·04)	0·47(0·02)	0·18(0·02)	0·84(0·02)	0·33(0·03)	0·09(0·01)	0·16(0·02)	0·44	0·42(0·02)	nd
CO_2 (p.p.m.)[y]	0	0	0	0	306 (9)	293 (20)	0	72 (7)	0	125 (8)	204 (16)	197 (15)	62 (6)	64 (6)	223 (16)
(μmol)	0	0	0	0	0·7	0·6	0	0·1	0	0·3	0·5	0·2	0·1	0·1	0·4

(continued on next page)

Table 1: continued

Experiment no.	7	8	9	17H	17M	18M	20H	20M	21H	21M	32A	33A	33B	34B	35B
Mole fractions and fugacities															
$X^{v}_{H_2O}$	1	1	1	1	0·028[u]	0·399[s]	1	0·387[t]	1	0·405[t]	0·134[u]	0·226[u]	0·582[u]	0·552[u]	0·035[u]
$X^{v}_{CO_2}$	0	0	0	0·972[u]	0·601[s]	0	0·613[t]	0	0·595[t]	0·866[u]	0·774[u]	0·418[u]	0·448[u]	0·965[u]	
f_{H_2O}[z]	205	200	298	709	17	377	308	116	503	196	62	106	287	271	16
f_{CO_2}[z]	0	0	0	0	815	690	0	201	0	331	489	435	228	245	546
$100{\cdot}X^{m}_{H_2O,mol}$[aa]	0·54	0·73	1·07	1·82	0·05	1·03	0·94	0·35	1·69	0·67	0·19	0·33	0·89	0·84	n.d.
$100{\cdot}X^{m}_{OH}$[aa]	3·62	3·86	4·61	7·26	1·51	5·67	4·48	3·59	5·28	4·22	2·92	2·87	4·95	5·09	1·91
$100{\cdot}X^{m}_{B}$[aa]	2·35	2·67	3·37	5·44	0·80	3·86	3·18	2·15	4·33	2·78	1·65	1·77	3·36	3·38	0·95
$100{\cdot}X^{m}_{CO_2}$[aa]	0	0	0	0	0·026	0·024	0	0·006	0	0·010	0·017	0·016	0·005	0·005	0·019

[a]Basaltic glass from sample TT152-21-35 (see Table 2) was powdered, pressed into pellets, and held at 940°C for 14 h at 1 atm in a CO_2–CO gas mixture corresponding to the quartz–fayalite–magnetite (QFM) buffer and then repowdered. [b]Powdered TT152-2-35 glass (not baked) having an initial H_2O content of 0·36 wt % (Dixon *et al.*, 1988). [c]Glass from sample TT152-51-3 was powdered and held in a Pt crucible at 900°C for 36 h in an H_2–CO_2 gas mix corresponding to the nickel–nickel oxide (Ni–NiO) buffer. [d]Fe loss controlled by double-capsule technique (see Van der Laan & Koster van Groos, 1991). [e]No Fe-loss control; runs performed in pure Pt capsules. [f]Initial concentration of Fe in Fe–Pt alloy calculated by mass balance after Fe plating and annealing of foils. [g]Fe in Pt-foils after the experiment determined by electron microprobe. Standards used were pure Pt and Fe metals. Backgrounds were 0·01 wt % for Fe in Pt and 0·05 for Pt in Fe. Total instrument precision is ~1% based on replicate analyses of standards of assumed purity. [h]f_{O_2} calculated using Gudmundsson & Holloway (1993) assuming equilibrium between FeO in the melt and Fe in the Fe–Pt alloy. [i]$\Delta QFM = \log_{10} f_{O_2}$ (sample) $- \log_{10} f_{O_2}$(QFM) at 1200°C, where $\log_{10} f_{O_2}$ (QFM) = –8·47 at 1200°C (Huebner, 1971). [j]f_{H_2} in Ar–H_2 gas mixture monitored using Shaw membrane. [k]f_{H_2} assumed from initial concentration of H_2 in pre-mixed Ar–H_2 pressurizing gas. [l]Pure Ar used as pressurizing gas. [m]f_{O_2} calculated using the standard free energies of formation of H_2O, H_2 and O_2 (JANAF, 1986) to calculate the equilibrium constant for the reaction $H_2 + \frac{1}{2}O_2 \times H_2O$ and an MRK equation of state (Holloway, 1987) for the fugacities of H_2O and H_2. [n]Total iron as FeO determined by electron microprobe using 15 kV accelerating potential, 15 nA beam current and 20 μm spot size. Standards used for the glass analyses were basaltic glass (VG-2) for Mg, Al, Si, Ca and Fe; synthetic TiO_2 for Ti; a synthetic Mn-olivine for Mn; Amelia albite for Na; and asbestos microcline for K. Data reduction was done using the CITZAF program (Armstrong, 1988), employing the absorption correction of Armstrong (1982), the atomic number correction of Love *et al.* (1978), and the fluorescence correction of Reed (1965) as modified by Armstrong (1988). [o]Ferrous iron determined by wet-chemistry by Professor Ian Carmichael (Lange & Carmichael, 1989). [p]Ferric iron determined by mass balance: $Fe_2O_3 = (FeO^* - FeO)/0{\cdot}9$. [q]Oxygen fugacities calculated using Kilinc *et al.* (1983) based on ferric–ferrous ratio in the glass. [r]Glass densities calculated based on melt composition after the experiment using Gladstone–Dale rule and the Church–Johnson equation as described by Silver *et al.* (1990). [s]Final vapor composition calculated by mass balance: amount of H_2O in final vapor = amount of initial water vapor + amount of initial dissolved water – amount of final total dissolved water; amount of CO_2 in final vapor = amount of initial CO_2 vapor – amount of final dissolved CO_2. Errors in parentheses for final amount of water vapor are limited by error in total dissolved water. Errors for final amount of CO_2 vapor are negligible because of small concentrations of dissolved CO_2. [t]Final vapor composition measured using manometry (see text). [u]Final vapor composition calculated using the measured concentration of molecular water and equation (2) to determine f_{H_2O} and an MRK equation of state for H_2O–CO_2 mixtures (Holloway, 1977) to determine f_{CO_2}, $X^{v}_{H_2O}$ and $X^{v}_{CO_2}$. Runs 32–35 are assumed to be closed with respect of CO_2, but open with respect to H_2 because of diffusion through Pt capsule. [v]Total water concentrations calculated using absorbances from 3530 cm^{-1} band and $\varepsilon^{3530} = 63 \pm 3$ l/mol-cm. Values in parentheses are 1σ standard deviations. [w]Wt % water dissolved as OH calculated from the absorbance of the 4500 cm^{-1} band using $\varepsilon^{4500} = 0{\cdot}67 \pm 0{\cdot}03$ l/mol-cm. Values in parentheses same as in v. [x]Concentrations of molecular H_2O calculated using the 5200 cm^{-1} band absorbances and $\varepsilon^{5200} = 0{\cdot}62 \pm 0{\cdot}07$. Values in parentheses same as in v. [y]Concentrations of dissolved carbonate calculated from 1515 and 1430 cm^{-1} band absorbances using $\varepsilon = 375$ l/mol-cm. Values in parentheses are 1σ standard deviations. [z]Fugacities calculated using a modified Redlich–Kwong equation of state for H_2O–CO_2 mixtures (Holloway, 1977). [aa]Mole fractions of volatile components calculated using: X^{m}_{B}(bulkwater) = {(wt %$H_2O^{sum}_{tot}$/18)/[(100 – wt %$H_2O^{sum}_{tot}$)/36·594 + wt %$H_2O^{sum}_{tot}$/18 + wt %CO_2/44]}, where wt %$H_2O^{sum}_{tot}$ = wt %OH + wt %H_2O_{mol}; $X^{m}_{OH} = 2(X_B - X^{m}_{H_2O,mol})$; $X^{m}_{H_2O,mol}$ = {(wt %H_2O_{mol}/18)/[(100 – wt %H_2O_{tot})/36·594 + wt %H_2O_{tot}/18 + wt %CO_2/44]}; and $X^{m}_{CO_2}$ = {(wt %CO_2/44)/[(100 – wt %H_2O – wt %CO_2)/36·594 + wt %H_2O/18 + wt %CO_2/44]}, where 36·594 is the molecular weight of anhydrous basalt on a single-oxygen basis. n.a., not analyzed; n.d., not detected.

Table 2: Composition of starting materials

Oxide	TT152-21-35[a] (wt%)	TT152-51-3[b] (wt%)
SiO_2	50·8	49·7
Al_2O_3	13·7	14·4
TiO_2	1·84	1·58
FeO*	12·4	11·30
MgO	6·67	7·14
CaO	11·5	12·31
Na_2O	2·68	2·93
K_2O	0·15	0·16
P_2O_5	0·19	0·11
MnO	0·22	0·18
S	0·15	n.a.
Total	100·4	100·00

[a]Microprobe analysis by Delaney & Karsten (in preparation). Same sample as used by Stolper & Holloway (1988).
[b]Microprobe analysis from Pawley *et al.* (1992). Same sample as used by Pawley *et al.* (1992).

a high surge current from a discharging capacitor to burn out the Pt-hanging wire, allowing the sample to drop to the bottom of the vessel (25°C) and achieving quench rates of ~500°C/s. All runs quenched to glass successfully.

ANALYTICAL TECHNIQUES

Electron microprobe

Most quenched glasses were analyzed by electron microprobe at the California Institute of Technology using a JEOL JXA-33 Superprobe. Concentrations of Fe and Pt in some Fe–Pt foils inserted in the Pt capsules to minimize iron loss were also determined after the experiments by electron microprobe. Analytical procedures, standards and correction procedures for electron microprobe analyses are described in the footnotes to Table 1.

Fe^{3+}/Fe^{2+}

Ferrous iron concentrations in the quenched glasses were measured by Professor Ian Carmichael at the University of California at Berkeley by a colorimetric, wet-chemical method (Wilson, 1960) corrected for time-dependent, ferric iron interference (Lange & Carmichael, 1989). Precision of the ferrous iron analyses is ~2% of the amount present based on multiple analyses of an internal laboratory standard [JDFD-2; 10·93 ± 0·21% (2σ)]. Ferric iron concentrations were determined by difference between the total iron as FeO (FeO*) based on the electron microprobe and the amount of ferrous iron (see caption to Table 1).

Manometry

The composition of the quenched H_2O–CO_2 vapor phase was measured in two runs (Nos 20M and 21M) using manometry (Ihinger, 1991), by P. Ihinger at Caltech. Capsules were pierced under vacuum at room temperature. Vapor was extracted in a series of cycles of expansion of the gas into an evacuated volume followed by condensation in a liquid nitrogen trap. After pumping away a small volume of non-condensable gas (~7 μmol or <4% of the total extracted vapor), the CO_2 was released by bathing the trap in a slurry of dry ice and M17 and transferred with a Toepler pump into a calibrated volume for manometric analysis. The water remaining in the

cold trap was evaporated and converted to H_2 by exposure to hot uranium (Bigeleisen *et al.*, 1952), then transferred with a Toepler pump to a calibrated volume for manometric analysis. Analytical uncertainty of the manometric measurements of the mass fractions of water and carbon dioxide in the vapor are estimated to be <0·01 (Ihinger, 1991).

IR spectroscopy

Data collection

Dissolved water and carbonate concentrations were determined by transmission IR spectroscopy on doubly polished glass chips, following in general the procedures and calibrations described by Dixon *et al.* (1988). At least three glass fragments from each experiment were polished for spectroscopic analysis. Samples were analyzed using the microchamber attachment to the Nicolet 60SX FTIR spectrometer using a Globar source, KBr beamsplitter and a $HgCdTe_2$ detector for the IR region and a W source, CaF_2 beamsplitter and an InSb detector for the near-IR region. A typical spectrum in the IR region (1500–3800 cm^{-1}) is shown in Fig. 1a and in the near-IR region (3500–6000 cm^{-1}) in Fig. 1c.

Total dissolved water was measured using the intensity of the broad asymmetric band centered at 3530 cm^{-1} corresponding to the fundamental OH-stretching vibration (Scholze, 1959; Nakamoto, 1978) using a molar absorptivity of 63 ± 3 l/mol-cm (P. Dobson, S. Newman, S. Epstein, & E. M. Stolper, unpublished data). The value of ε^{3530} has been independently determined recently by Pandya *et al.* (1992*a*) to be 61 ± 1, the same, within 1σ error, as our value. The background under the 3530 cm^{-1} band was assumed to be linear between 3800 and 2500 cm^{-1}.

Concentrations of water dissolved as molecular water were measured using the intensity of the 5200 cm^{-1} band, resulting from the combination stretching + bending mode of water molecules (Scholze, 1960; Bartholomew *et al.*, 1980). Concentrations of water dissolved as hydroxyl groups were measured using the intensity of the 4500 cm^{-1} band, resulting from combination modes for X–OH (X = Si, Al, etc.) groups (Scholze, 1966; Stolper, 1982*a*). Calibration of the molar absorptivities of the 5200 and 4500 cm^{-1} bands for basaltic glasses is discussed in the Results and Discussion ('Calibration of ε^{4500} and ε^{5200}'). The near-IR background was modeled as a sum of 5 Gaussians: one each for the Fe absorptions centered at about 9500 and 5500 cm^{-1} corresponding to the crystal-field transitions in octahedrally and tetrahedrally coordinated Fe^{2+} ions (Bell *et al.*, 1976; Goldman & Berg, 1980), one centered at ~4000 cm^{-1} to fit an unassigned water-related band (Stolper, 1982*a*), and two to fit the high-energy shoulder of the 3530 cm^{-1} absorption. A non-linear curve fitting routine was used to fit the intensities, position

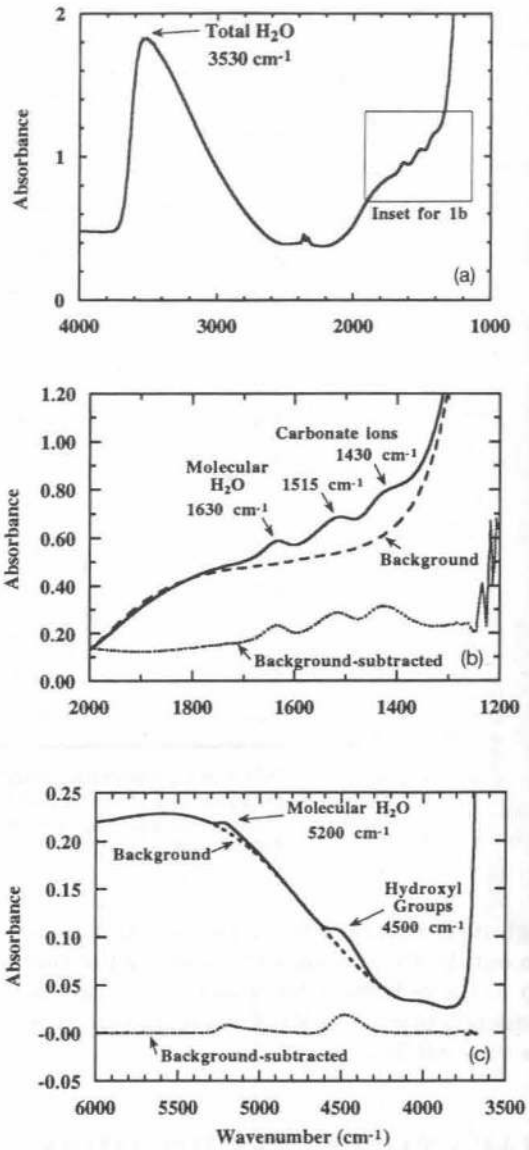

Fig. 1. (a) Infrared spectrum of basaltic glass from experiment No. 32A (thickness 179 μm) showing typical absorptions of total water (3530 cm^{-1}), molecular water (1630 cm^{-1}) and carbonate bands (1515 and 1430 cm^{-1}). Small peaks at ~2350 cm^{-1} are absorptions by atmospheric CO_2. (b) Enlargement of 1200–2000 cm^{-1} region of (a) showing absorptions of molecular water and carbonate bands. Background used was spectrum of devolatilized basaltic glass (dashed line). The background-subtracted spectrum (dotted line) is also shown. The vertical positions of the spectra have been adjusted to allow easy comparison of the spectra. (c) Typical near-IR spectrum and background-subtracted spectrum of basaltic glass from experiment No. 9 (thickness 153 μm) showing the absorptions of molecular water at 5200 cm^{-1} and hydroxyl groups at 4500 cm^{-1}. Background modeled as described in text.

and half-widths of these background components (Bevington, 1969; Program 11-5, p. 237). This method is similar to that used by Stolper (1982*a*), except that he fitted the high-energy shoulder of the 3530 cm^{-1} band with a Lorentzian instead of two Gaussians. A typical spectrum, the modeled fit and the resulting background-subtracted spectrum are shown in Fig. 1c. (Note the flat background on the background-subtracted spectrum and the characteristic asymmetric shapes of the 5200 and 4500 cm^{-1} bands.) Peak heights were measured from the background-subtracted spectra. For comparison with the values measured using the 5200 cm^{-1} band, concentrations of water dissolved as molecular water were also measured using the band at 1630 cm^{-1}, corresponding to the fundamental bending mode of dissolved water molecules (Nakamoto, 1978). Calibration of the molar absorptivity of the 1630 cm^{-1} band for basaltic glasses is discussed in the section 'Calibration of ε^{4500} and ε^{5200}'.

Dissolved carbonate was measured from the intensities of the bands at 1515 and 1430 cm^{-1} corresponding to antisymmetric stretching of distorted carbonate groups (Brey & Green, 1975; Sharma, 1979; Sharma *et al.*, 1979; Fine & Stolper, 1986) using a molar absorptivity of 375 l/mol-cm (Fine & Stolper, 1986). Figure 1b shows for the carbonate region the spectra of a typical sample and of a decarbonated basaltic glass reference; also shown is the difference between these two spectra. The shape of the background in the region of the carbonate doublet is a complex and not fully understood function of composition; therefore, the reference-subtracted spectrum is typically not as flat as in the near-IR region and some subjective adjustment of the background was often required. Peak heights of both maxima on the carbonate doublet were measured separately on the background-subtracted spectra.

Precision and accuracy of spectroscopic data

The precision of the spectroscopic measurements is estimated from multiple analyses of a single spot on a glass fragment and is dominated by error introduced by the background correction. The precision of measurements of total water based on measurement of the 3530 cm^{-1} band using either the $HgCdTe_2$ or InSb detector is $\sim$2% (1σ). When the 3530 cm^{-1} band was analyzed on the same spot using both the $HgCdTe_2$ and InSb detectors, however, the measurements made using the InSb detector were sometimes higher by as much as 14%. Water concentrations reported in Table 1 are averages of all individual measurements, regardless of the detector used. The precision of molecular water, hydroxyl group and carbonate group analyses based on multiple analyses of the same spot is estimated to be $\sim$5–10%. Accuracies are limited by the uncertainties in the molar absorption coefficients and in the background correction procedures, and are estimated to be 10% for total water and 15% for carbonate (Dixon *et al.*, 1988). Uncertainties in the molar absorption coefficients for molecular water and hydroxyl groups are discussed in the section 'Calibration of ε^{4500} and ε^{5200}'.

RESULTS AND DISCUSSION

Run products

Conditions of all successful experiments are listed in Table 1. Run products were mostly transparent, brown to reddish brown glass. Glass at the bottoms of the capsules of the CO_2-rich experiments was a milky, bluish green color caused by streaks of silver from the breakdown of silver oxalate (Fine & Stolper, 1985). Most samples had bubbles (10–1000 μm) concentrated along the capsule walls, resulting in 'dimples' as described by Burnham & Jahns (1962) and by Hamilton *et al.* (1964). Several run products had a single large (1–2 mm) bubble in the center of the quenched glass.

Major element composition, Fe loss and oxidation state

Homogeneity of quenched glasses for each starting composition is about $\pm$1% for major elements, $\pm$2–3% for the minor elements and $\pm$5% for FeO*. Measured oxide concentrations, except for TiO_2 and FeO*, are within $\pm$7% of the published values for the starting materials (Table 2). Measured TiO_2 concentrations are up to 11% lower than the published values. Variations in FeO* contents (Table 1) are discussed in the next paragraph. The mean Fe contents of the Pt–Fe foils are similar to their initial values (Table 1), but there is typically some variability resulting from reaction with the melt during the runs.

FeO*, FeO and Fe_2O_3 contents of quenched glasses are listed in Table 1 along with oxygen fugacities calculated from the Fe^{3+}/Fe^{2+} of the glasses using the relationships of Kilinc *et al.* (1983). Glasses from experiments in which Pt–Fe alloy inserts (Nos 7–21; all done with starting material TT152-21-35) were used to minimize iron loss have total iron contents of 11·4–13·1 wt %, within 8% of the initial iron content of 12·4 wt %. Based on their Fe^{3+}/Fe^{2+} (0·17–0·82), these glasses are more oxidizing than the QFM buffer (ΔQFM = +0·4 to

+3·5). Glasses from experiments done in pure Pt capsules (Nos 32–35; all done with starting material TT152-51-3) have total iron contents of 10·1–10·4 wt %, within 11% of the initial iron content of 11·3 wt %. These runs are generally highly oxidized (ΔQFM = +2·6 to +9·7; Fe^{3+}/Fe^{2+} = 1·5–19·6), and are reddish brown because of their high Fe^{3+}/Fe^{2+}. Several factors contributed to the more oxidizing conditions of these experiments: (1) more oxidized starting material (see footnote to Table 1); (2) greater amounts of Fe loss to the Pt capsule, which releases oxygen; (3) H_2 loss from the capsule to the pure Ar pressurizing medium during the run. FeO concentrations for two glasses from the experimental study of Stolper & Holloway (1988) were also analyzed (Nos TT152-2 and TT152-5); they also indicate oxygen fugacities >QFM (ΔQFM = +0·4 to +1·8; Fe^{3+}/Fe^{2+} = 0·17–0·36).

Knowledge of the oxygen fugacity in our experiments is critical as it allows us, given knowledge of hydrogen fugacity or a constraint either on the C:H or C:O ratio of the vapor, to calculate the speciation of the vapor phase under the run conditions (Eugster & Skippen, 1967; Holloway *et al.*, 1968; Holloway & Reese, 1974; Pawley *et al.*, 1992). In particular, the high oxygen fugacities of our experiments (>QFM) at 1200°C indicates that <2% of the hydrogen in the vapor is in species other than H_2O and that <5% of the carbon in the vapor is in species other than CO_2 (e.g. CO); i.e. given these values for oxygen fugacity, the vapor phase in our experiments can be approximated as an H_2O–CO_2 fluid. The similarly high oxygen fugacities for the experiments of Stolper & Holloway (1988) also indicate, contrary to the suggestion of Pawley *et al.* (1992), that discrepancies between their results and those of Stolper & Holloway for CO_2 solubility in basalt are not the result of significant quantities of CO in the vapor phase of the Stolper & Holloway experiments.

Though we achieved our goal of maintaining oxygen fugacities more oxidizing than QFM, our attempts to control f_{O_2} through the use of premixed Ar–H_2 pressurizing gas appear to have been unsuccessful; i.e. there is no correlation between oxygen fugacities based on the measured Fe^{3+}/Fe^{2+} of the glasses and those calculated assuming an f_{H_2} in the capsule the same as that in the pressurizing gas. The reason for this is not clear, as this technique has been shown to provide an 'infinite reservoir' of known, constant f_{H_2} for the duration of the experiments on H_2O–CO_2–NaCl fluids (Joyce & Holloway, 1993). Also, we note that there is no correlation between oxygen fugacities calculated based on the Fe^{3+}/Fe^{2+} of the glasses and those based on the initial Fe content of the Pt–Fe alloy inserts and the FeO content of the glasses (Gudmundsson & Holloway, 1993).

Determination of molar absorptivities for the 4500 and 5200 cm^{-1} bands

Calibration of ε^{4500} *and* ε^{5200}

Molar absorptivites for the 4500, 5200 and 1630 cm^{-1} bands were determined using a procedure similar to that of Newman *et al.* (1986). We assumed that the molar absorptivities for the 3530, 4500 and 5200 cm^{-1} bands are constant and that all water is dissolved as either hydroxyl groups or molecules of water that absorb at these energies. This leads to the following relation [analogous to equation (2) of Newman *et al.* (1986)] among the absorption coefficients (i.e. absorption per unit thickness, or Abs/cm) of the various bands and their molar absorptivities (ε):

$$\frac{\varepsilon^{3530}}{\varepsilon^{5200}}\cdot(\mathrm{Abs/cm})^{5200}+\frac{\varepsilon^{3530}}{\varepsilon^{4500}}\cdot(\mathrm{Abs/cm})^{4500}=(\mathrm{Abs/cm})^{3530} \quad (1)$$

where the superscripts refer to the wavenumbers of the specific bands. We used all spectra for which intensities of the 5200, 4500 and 3530 cm^{-1} bands were measured (53 spots, 53 spectra) to determine best fit values for the ratios $\varepsilon^{3530}/\varepsilon^{5200}$ and $\varepsilon^{3530}/\varepsilon^{4500}$. Values for ε^{5200} and ε^{4500} were then determined using the value of $\varepsilon^{3530} = 63 \pm 3$ (1σ) l/mol-cm (P. Dobson, S. Newman, S. Epstein & E. M. Stolper, unpublished data). Similarly, we used all spectra for which intensities of the 5200 and 1630 cm^{-1} bands were measured on the same spot in the IR and near-IR regions (47 spots, 94 spectra) and determined the best fit Abs^{1630}/Abs^{5200} ratio, equal to the $\varepsilon^{1630}/\varepsilon^{5200}$ ratio, which in conjunction with the ε^{5200} value determined as described above, gives ε^{1630}.

Best fit molar absorptivities determined in this study for basaltic melts are $0{\cdot}62 \pm 0{\cdot}07$ for ε^{5200}, $0{\cdot}67 \pm 0{\cdot}03$ for ε^{4500}, and 25 ± 3 for ε^{1630}. Uncertainty in the value of the molar absorptivities (~11% for molecular water and ~4% for hydroxyl groups) limits the accuracy of analyses for these species. Moreover, care must be taken when applying these values to apply background correction procedures similar to those we have employed; otherwise, systematic inaccuracies could result.

Compositional dependence of ε^{4500} *and* ε^{5200}

The best-fit molar absorptivities for molecular water and hydroxyl groups in basaltic glasses are compared with those for other silicate melt compositions in Table 3. Although other compositional variables

Table 3: Molar absorptivity calibration for molecular water and hydroxyl groups

No.	Composition	Cation Fraction $Si^{4+}+Al^{3+}$	Molecular water Position (cm^{-1})	Molecular water ε (l/mol-cm)	Molecular water Position (cm^{-1})	Molecular water ε (l/mol-cm)	Hydroxyl groups Position (cm^{-1})	Hydroxyl groups ε (l/mol-cm)
1	MORB[a]	0·63	5200	0·62±0·07	1630	25±3	4500	0·67±0·03
2	$Na_2O·3SiO_2$[b]	0·60	5236	0·634			4505	0·267
3	NKZAS[c]	0·69	5236	1·00±0·08	~1630	28±5	4505	0·55
4	CAS–E2[d]	0·77	5204	1·07±0·04			4485	0·85±0·03
5	Jadeite[d]	0·75	5207	1·13			4476	1·12
6	Albite[e]	0·80	5218	1·67±0·06	1636	49±2	4485	1·13±0·04
7	KAS[d]	0·80	5222	1·87±0·07			4472	1·43±0·05
8	Rhyolite[f]	0·86	5225	1·86±0·05	1630	55±2	4503	1·50±0·10
9	Fused silica[g]	1·0						3·9

[a]This study; errors (1σ) were propagated from errors on the best-fit $\varepsilon^{3530}/\varepsilon^{5200}$, $\varepsilon^{3530}/\varepsilon^{4500}$, $\varepsilon^{3530}/\varepsilon^{1630}$ and $\varepsilon^{1630}/\varepsilon^{5200}$ ratios and on the error for the value of ε^{3530} (63±3 l/mol-cm). [b]Acocella *et al.* (1984). [c]NKZAS is Na_2O–K_2O–ZnO–Al_2O_3–SiO_2 glass; Bartholomew *et al.* (1980). [d]CAS-E2 are two different calcium–aluminosilicate glass compositions; KAS is orthoclasic glass; Silver *et al.* (1990). [e]Silver & Stolper (1989). [f]P. D. Ihinger (personal communication). [g]Estimated from ε^{3670} = 181 l/mol-cm (Shelby *et al.*, 1982) and an $\varepsilon^{4500}/\varepsilon^{3670}$ of 0·022 (Stolper, 1982*a*). The ε^{4500} estimated in this way is significantly higher than a previously reported value of 1·75 l/mol-cm by Dodd & Fraser (1966).

clearly influence the values of the molar absorptivities, both ε^{4500} and ε^{5200} correlate positively and linearly ($R^2 = 0·87$ and 0·86, respectively) with the sum of the concentrations (cation fractions) of Si and Al (Fig. 2a and b). It should be noted that fused silica glass differs spectroscopically from the other glasses shown in Fig. 2 (McMillan & Remmele, 1986); the deviation in Fig. 2b of silica from the simple trend established by the other compositions may reflect these differences. The relationships shown in Fig. 2 may help to predict the molar absorptivities of hydrous species in glasses when they have not been measured directly, but we emphasize that, for quantitative work, it is critical to determine the molar absorptivities for each composition of interest. These systematic variations in molar absorptivity probably reflect relationships between hydrous species and aluminosilicate units in glasses and may ultimately provide useful tests of models of chemical and structural interactions between these species and the major components of the glass structure. However, the key point for this paper is that the systematic compositional dependence shown by molar absorptivities determined in several laboratories on a range of glass compositions gives us confidence in our calibration of the IR spectroscopic technique for determining concentrations of hydrous species in silicate glasses.

Uncertainties in spectroscopic data

Concentrations of total dissolved water, water dissolved as water molecules and as hydroxyl groups, and carbon dioxide dissolved as carbonate are listed in Table 1. Uncertainties (1σ of all analyses from that run) cited in Table 1 reflect both precision and homogeneity and are usually slightly greater than the analytical precision. For total water concentrations, all individual measurements are averaged, regardless of detector used. Uncertainties in total water concentrations are typically 2–8% of the amount present, but in one case the uncertainty is 13%. Uncertainties in species concentrations are <11% for molecular water, <13% for hydroxyl groups and <10% for carbonate groups.

Speciation of water in MORB glasses

Concentrations of molecular water and hydroxyl groups in the 15 MORB glasses synthesized in this study are shown versus total water concentration in Fig. 3a. Molecular water concentrations based on the 5200 and 1630 cm^{-1} bands are essentially identical; for simplicity, only results based on the 5200 cm^{-1} band are shown. Figure 3b compares the speciation data for basaltic glasses from this study and albitic glasses quenched from 1400°C (Silver & Stolper, 1989). When plotted in terms of mole frac-

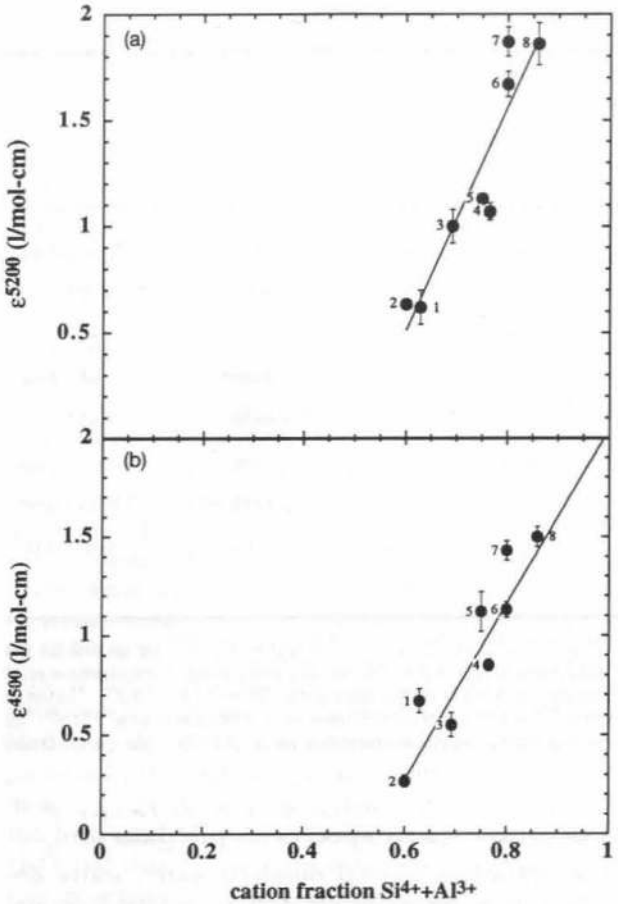

Fig. 2. Compositional dependence of molar absorptivities for (a) molecular water (5200 cm^{-1} band) and (b) hydroxyl groups (4500 cm^{-1} band). Molar absorptivities for both bands correlate linearly with the cation fraction of tetrahedral cations (T), where $T = (Si^{4+} + Al^{3+})/(\text{total cations})$. Sources of data and key numbers are listed in Table 3. The molar absorptivity for the 4500 cm^{-1} band for fused silica ($T = 1$, $\varepsilon^{4500} = 3{\cdot}9$) was not included in the fit (see text). Weighted linear fits through the data are $\varepsilon^{5200} = -2{\cdot}6 + 5{\cdot}1T$ and $\varepsilon^{4500} = -2{\cdot}3 + 4{\cdot}4T$.

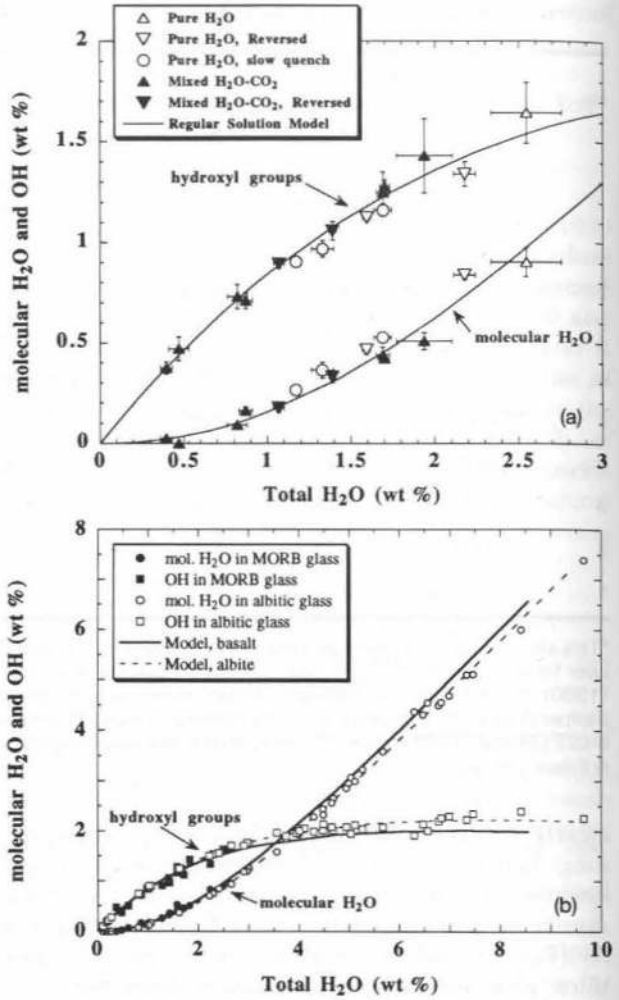

Fig. 3. (a) Concentrations of water dissolved as molecular H_2O and as OH groups as functions of total water (measured using 3530 cm^{-1} band) for MORB melt equilibrated with pure H_2O vapor or mixed H_2O–CO_2 vapor at 1200°C. Slow quench samples (open circles) were run in conventional IHPV and quenched at rate of 8°C/s. All other runs quenched at ~500°C/s in rapid-quench IHPV. Speciation model curves for basaltic glass are calculated using a regular solution model for albitic glass (see caption to Table 5), where the activity of water in the melt is given by Henry's law for molecular water [equation (2)]. Errors are 1σ from Table 1. (b) Concentrations of water dissolved as molecular H_2O (circles) and as OH groups (squares) as functions of total water (sum of mol H_2O and OH) for MORB and albitic glasses. Albitic glass samples synthesized in piston cylinder apparatus at 1400°C; data from Silver & Stolper (1989). MORB data from this study. Curves are calculated as described in (a) above. The small differences between the two sets of curves reflect the different values of molecular weight per oxygen of basaltic (36·594 g/mol) and albitic (32·78 g/mol) glasses. If plotted in terms of mole fractions, the two model curves in Fig. 3b are nearly coincident.

tions on a single oxygen basis, the data for basaltic and albitic glasses are indistinguishable. Also shown in Fig. 3a and b is a regular solution model calculated using the best-fit coefficients for albitic glass (Silver & Stolper, 1989; see caption to Table 5). Concentrations of molecular water and hydroxyl groups over a range of total water contents based on the regular solution model are listed in Table 5 below.

Molecular water concentrations in glasses from this study range from 0 to 0·90 wt %. Concentrations of hydroxyl groups range from 0·47 to 1·85 wt %. At the low total water concentrations of these experiments, water dissolves in the glass dominantly as hydroxyl groups. As the total concentration of water increases, the concentration of hydroxyl groups begins to level off, and a larger and larger fraction of the water dissolves as molecular water. By analogy with the albitic glass, beyond ~3·5 wt % total water, molecular water is expected to become the dominant form of dissolved water. The trends in

water speciation in quenched MORB glasses are similar to those observed for other hydrous silicate glasses measured using IR spectroscopy (Bartholomew *et al.*, 1980; Wu, 1980; Stolper, 1982*a*, *b*, 1989; McMillan *et al.*, 1983; Towozawa *et al.*, 1983; McMillan & Remmele, 1986; Silver & Stolper, 1989; Silver *et al.*, 1990; Ihinger, 1991).

NMR spectroscopic studies have yielded similar quantitative results (Bartholomew & Schreurs, 1980; Eckert *et al.*, 1989; Kohn *et al.*, 1989), but Raman spectroscopic measurements have been interpreted as indicating that the ratio of molecular water to hydroxyl groups is independent of total water content and that the abundance of hydroxyl groups increases with total water contents (Mysen & Virgo, 1986; Mysen, 1992). The reason for the significant differences between the results of IR and NMR spectroscopic measurements on the one hand and the Raman measurements on the other is unknown. However, we note that the quantification of the IR measurements is straightforward (i.e. the band assignments for OH vs H_2O are uncontroversial; the bands are non-overlapping and readily resolvable; Beer's law has been shown to be valid for all the relevant bands; and there is redundancy in the results through comparison of the intensities of mid- and near-IR bands reflecting the same H-bearing species) and that it would be difficult to reconcile the results of this or any previous IR studies with the constant ratio of molecular water to hydroxyl (or total water) inferred by Mysen & Virgo (1986) and Mysen (1992).

There is no detectable difference in the proportions of molecular water and hydroxyl groups in the slow (conventional IHPV) and fast (rapid-quench IHPV) quench experiments (Fig. 3a). This is similar to observations for albitic (Silver & Stolper, 1989) and Ca–Al–silicate (Silver *et al.*, 1990) glasses, but contrasts with those for rhyolitic glasses in which a similar range of quench rates led to measurable differences in speciation (Silver *et al.*, 1990; Ihinger, 1991). Following the treatment of Dingwell & Webb (1990), that quench rates different by two orders of magnitude do not lead to detectable differences in the speciation of water in basaltic glasses suggests either that water speciation in these compositions is not temperature dependent in the vicinity of the glass transition, or that the simple treatment they present is inadequate to deal with these complex systems. Although we do not know the significance of the apparent independence of our speciation results from quench rate, it is interesting that the dependence of speciation on quench rate appears to be strongest in the most silica-rich composition yet investigated.

Based on a study of basaltic to dacitic submarine glasses from Hawaii, Pandya *et al.* (1992*a*) concluded that the speciation of water in silicate melts is a strong function of melt composition (i.e. wt % SiO_2). In particular, they observed a factor of 10 increase in the ratio of the absorbance of the 1630 cm^{-1} band to the 3530 cm^{-1} band when the total water content increased from 0·55 to 1·74 wt % and the silica content increased from 49 to 64 wt %. They concluded that at constant total water content, the fraction of water dissolved as molecular water increases significantly with silica content. In contrast, our results (Fig. 3b) and previous studies (Silver & Stolper, 1990) show only a minor dependence of the speciation of water on the anhydrous glass composition. However, Pandya *et al.* (1992*a*) did not take into account that the molar absorptivities for hydrous species in these glasses are strong functions of glass composition (see Table 3) and thus that direct comparison of absorbance ratios can be misleading. Indeed, using the relationship between composition and ε^{5200} shown in Fig. 2 and assuming a constant $\varepsilon^{1630}/\varepsilon^{5200}$, we calculate that rather than being constant as they assumed, ε^{1630} increases by a factor of 1·8 over the range of compositions studied by Pandya *et al.* (1992*a*). When molecular water concentrations in the samples studied by Pandya *et al.* (1992*a*) are recalculated using this compositional dependence of ε^{1630}, most correspond well to the relationship illustrated in Fig. 3 for MORB and albitic glasses.

A few of the glasses studied by Pandya *et al.* (1992*a*) have molecular water contents greater than expected based on our results, even after correction for the compositional dependence of ε^{1630}, although the magnitude of the excess is not a function of SiO_2 content. Glasses hydrated experimentally at low temperature contain anomalously high concentrations of molecular water (Olbert & Doremus, 1983; Pandya *et al.*, 1992*b*) consistent with a model in which molecular water is the diffusing species and the interconversion of H_2O to OH is slow at low temperatures (Zhang & Stolper, 1991; Zhang *et al.*, 1991; Jambon *et al.*, 1992). Thus, one possible mechanism for producing these excesses is low-temperature hydration after submarine eruption. Hydration, caused by diffusion of water molecules, would precede the physical and chemical alteration of glass to palagonite. The speciation of water in submarine basaltic glasses may provide a means to discriminate 'fresh' glasses from those whose water contents have been modified by low-temperature processes (e.g. Clague *et al.*, 1991).

Although there is consensus that water dissolves in silicate melts and glasses as both water molecules

and hydroxyl groups, the reactions by which hydroxyl groups are formed by interaction between water molecules and the silicate matrix are not well understood [see discussions by McMillan & Holloway (1987) and McMillan (1994)]. For example, the extent of interaction in highly polymerized aluminosilicate melts between hydroxyl groups and TOT linkages (where T is Si or Al) is uncertain. The classic view is that reaction between water molecules and bridging oxygens breaks TOT linkages to form two T–OH groups (e.g. Buerger, 1948; Burnham, 1975; Stolper, 1982*b*; McMillan *et al.*, 1993; Sykes & Kubicki, 1993, 1994). An alternative view is that reaction of water molecules to form hydroxyl groups does not break a TOT linkage; instead, one hydrogen bonds to the bridging oxygen, thus weakening but not breaking the TOT linkage, and the remaining OH^- forms a hydrated complex such as $Na^+(OH^-)(H_2O)_n$ (Kohn *et al.*, 1989, 1992, 1994). In this second case, half of the OH^- groups in the glass would be present as hydrated complexes that would not contribute to the 4500 cm^{-1} combination band in the near-IR (Kohn *et al.*, 1992; Pichavant *et al.*, 1992). Although this latter reaction mechanism, if it applies to less polymerized structures such as basaltic melts and glasses, would affect the value of the molar absorptivity for the 4500 cm^{-1} band (as it would falsify the assumption that all H-bearing species contribute either to the 5200 or the 4500 cm^{-1} band), it would not affect the quantification of water speciation presented in this study provided that, as this model asssumes, the ratio of hydroxyl groups contributing to the absorption at 4500 cm^{-1} to those that do not is a constant. Thus, although the resolution of this controversy and its relevance to basaltic melts and glasses are essential to a full understanding of the influence of dissolved water on melt structure and properties, it has no direct impact on the results or conclusions of our study.

Solubility of water in MORB melts

Six successful experiments using pure water were conducted at 1200°C with total pressure ($\sim P_{H_2O}$ in these experiments) ranging from 200 to 717 bar. Three experiments (Nos 7, 8 and 9) were conducted in the conventional IHPV and three (Nos 17H, 20H and 21H) were conducted in the rapid-quench IHPV. Three successful experiments (Nos 18M, 20M and 21M) using oxalic acid dihydrate to produce a mixed H_2O–CO_2 vapor phase were conducted at 1200°C at total pressures ranging from 310 to 980 bar in the rapid-quench IHPV. Mole fractions of water and carbon dioxide in these H_2O–CO_2 vapors were determined by manometry or calculated by mass balance (see footnote to Table 1). The validity of the mass balance calculations was checked in the two samples (Nos 20M and 21M) in which the vapor compositions were determined directly by manometry; the calculated and measured mole fractions of H_2O in the vapor ($X^v_{H_2O}$) agreed to better than 0·01 (absolute). Additional mixed H_2O–CO_2 vapor experiments (Nos 32–35) were conducted, but the water content of the vapor could not be determined by mass balance because pure Ar was used as the pressurizing gas in these runs, leading to significant amounts of H_2 loss from the capsule.

Figure 4a shows the total dissolved water contents of quenched glasses from vapor-saturated experiments based on the intensity of the 3530 cm^{-1} band vs water fugacity [calculated using an MRK equation of state (Holloway, 1977)]. Total water concentrations range from 1·0 to 2·5 wt %. The water concentrations of runs No. 7 (1·28 ± 0·03 wt % H_2O, held at a total pressure of 206 bar for 2·5 h, $f_{H_2O} = 205$ bar) and No. 8 (1·43 ± 0·18 wt % H_2O, held at a total pressure of 400 bar for 2·25 h and then dropped to and held at 200 bar for 2·75 h, $f_{H_2O} = 200$ bar) agree within error. This reversal and the fact that other results that were approached both from above and below the final pressure bracket a smooth curve indicate that equilibrium was reached on the time scale of these experiments. The total water contents of runs No. 9 (run in the conventional IHPV, 1·74 ± 0·12 wt % H_2O, $f_{H_2O} = 298$ bar) and No. 20H (run in the rapid-quench IHPV, 1·71 ± 0·02 wt % H_2O, $f_{H_2O} = 308$ bar) differ by only 2%, showing that quench rate does not affect measured water solubility at these pressures. Also, the total dissolved water contents in these experiments do not appear to depend on f_{O_2} or the presence or absence of CO_2 in the vapor phase.

Figure 4b compares our results with those of Hamilton *et al.* (1964) for a Columbia River basalt at higher pressures, and shows that water solubility is not a strong function of melt composition for tholeiitic melts in this pressure range. Also shown are Russian data on water solubility in basaltic melts in equilibrium with pure H_2O vapor (Khitarov *et al.*, 1959) and mixed H_2O–CO_2 vapor (Kadik *et al.*, 1972). For pressures >2 kbar, these data are consistent with those of Hamilton *et al.* (1964). Below 2 kbar, however, the results of Kadik *et al.* (1972) in the mixed volatile system are systematically up to 40% lower than the data of Khitarov *et al.* (1959) in the basalt–H_2O system and than our data in the basalt–H_2O and basalt–H_2O–CO_2 systems. The solubility of water in MORB liquids is intermediate between those in orthoclasic and albitic liquids (Silver *et al.*, 1990) at 1200°C and pressures <5 kbar (Fig. 4c).

The dependence of the activity of water in vapor-saturated melt on total pressure and water fugacity at constant temperature (T_0, K) is given by the following expression (Silver & Stolper, 1989; Silver *et al.*, 1990):

$$a^{m}_{H_2O}(P, T_0) = a^{m}_{H_2O}(P_0, T_0)\frac{f_{H_2O}(P, T_0)}{f_{H_2O}(P_0, T_0)}\exp\left[\frac{-V^{o,m}_{H_2O}(P - P_0)}{RT_0}\right] \quad (2)$$

where $a^{m}_{H_2O}(P,T_0)$ is the activity of water in melt saturated with vapor with a fugacity of water of $f_{H_2O}(P,T_0)$ at pressure P and temperature T_0; $a^{m}_{H_2O}(P_0,T_0)$ is the activity of water in melt in equilibrium with vapor with a fugacity of water of $f_{H_2O}(P_0,T_0)$ at pressure P_0 and temperature T_0; $V^{o,m}_{H_2O}(P,T_0)$, taken to be a constant, is the molar volume of water in the melt in its standard state; and R is the gas constant.

The data shown in Fig. 4a and b can be evaluated in terms of equation (2) given an expression relating the concentration of water in the quenched melt to the activity of water in the melt. We choose a standard state for dissolved water in the melt equal to that for dissolved molecular water and adopt the approximation that the activity of molecular water can be described by Henry's law; i.e.

$$a^{m}_{H_2O}(P, T_0) = a^{m}_{H_2O\,molecules} \propto X^{m}_{H_2O\,molecules}. \quad (3)$$

Provided the molecular water concentrations of the quenched glasses are not significantly changed on quenching, the validity of the Henrian approximation can be evaluated by plotting water fugacity against the mole fraction of molecular water in glasses quenched from melts equilibrated with vapor at constant total pressure [the variation in water fugacity at constant total pressure is achieved by varying the composition of the vapor (Blank *et al.*, 1993*a*)]. In this case, the volume-dependent term drops out of equation (2) and activity is directly proportional to fugacity, so if the concentration of molecular water is proportional to water fugacity, it must also be proportional to activity. The same test can be carried out using solubility data from runs equilibrated with vapor over a range of low pressures provided the range of total pressures is sufficiently small that the

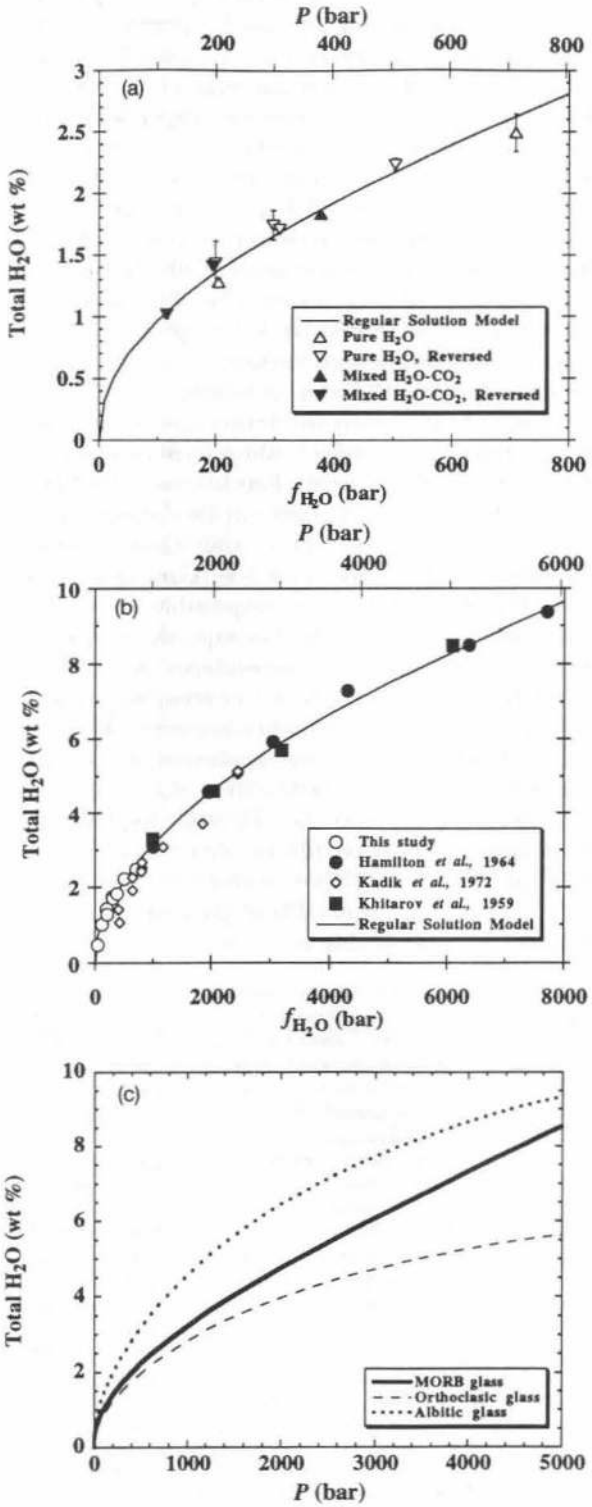

Fig. 4. (a) Total H_2O (wt% from 3530 cm^{-1} band) plotted against water fugacity for MORB liquids in equilibrium with 'pure' H_2O and mixed H_2O–CO_2 fluids. Errors in water concentration are 1σ from Table 1. Errors in water fugacity are smaller than the size of symbols. (b) Comparison of new experimental results for the solubility of H_2O (wt%) in MORB with previous results on basalt in equilibrium with pure water (Khitarov *et al.*, 1959; Hamilton *et al.*, 1964) and mixed H_2O–CO_2 vapor (Kadik *et al.*, 1972). Model curves in both (a) and (b) were calculated using a regular solution model for speciation of water with the coefficients for albitic glasses (Silver & Stolper, 1989; see caption to Table 5), where the activity of water in the melt is given by Henry's law for molecular water [equation (2)]. (c) Comparison of water solubility in basaltic melts with that in albitic and orthoclasic melts at 1200°C (Silver *et al.*, 1990).

pressure-dependent term in equation (2) can be neglected (Silver *et al.*, 1990).

Figure 5a shows the relationship between molecular water content and water fugacity for the H_2O- and H_2O–CO_2-saturated experiments from this study. The relationship is clearly Henrian. Using only the $P < 510$ bar data, the best-fit line (dotted in Fig. 5a) is $X^m_{H_2O} = 3{\cdot}2 \pm 0{\cdot}1 \times 10^{-5}$ f_{H_2O} ($R^2 = 0{\cdot}95$). The solid curves in Figs 4a and 5a show the calculated total and molecular water solubility (i.e. $P_{Total} = P_{H_2O}$) based on a best fit to equation (2) using our data and higher-pressure experiments from the literature (see next paragraph). It should be noted that although the results of the H_2O–CO_2-saturated experiments should be slightly displaced from the solid curves in Figs 4a and 5a (to lower total and molecular water contents for a given water fugacity) because of the pressure-dependent term in equation (2), in fact this effect is too small to be detectable at the low pressures of our experiments given the relatively small $V^{o,m}_{H_2O}$. The conclusion that the activity of molecular water can be described by Henry's law is an important one in that it means that spectroscopically measurable variations in the concentration of molecular water provide an accurate approximation to variations in the thermodynamic activity of water in basaltic melt. This has previously been shown to be the case for a range of more highly polymerized aluminosilicate compositions (Silver *et al.*, 1990; Blank *et al.*, 1993*a*) and appears to be a general result at low pressures.

By combining our data and those given by Hamilton *et al.* (1964) and Khitarov *et al.* (1959) from higher pressures, it is possible to obtain a value for $V^{o,m}_{H_2O}$, given the assumptions that $a^m_{H_2O} \propto X^m_{H_2O,mol}$ and that the dependence of molecular water content on total water content in water-rich basaltic melts from the higher-pressure experiments can be described by the extrapolation of the regular solution fit to the speciation data shown in Fig. 3. Taking $P_0 = 1$ bar and $T_0 = 1200°C$, we have fitted these data to equation (2) to obtain best fit values of $a^m_{H_2O}(1\text{ bar},\ 1200°C) = (3{\cdot}28 \pm 0{\cdot}06) \times 10^{-5}$ and $V^{o,m}_{H_2O} = 12 \pm 1$ cm^3/mol. These parameters yield an excellent fit to available solubility data, as shown in

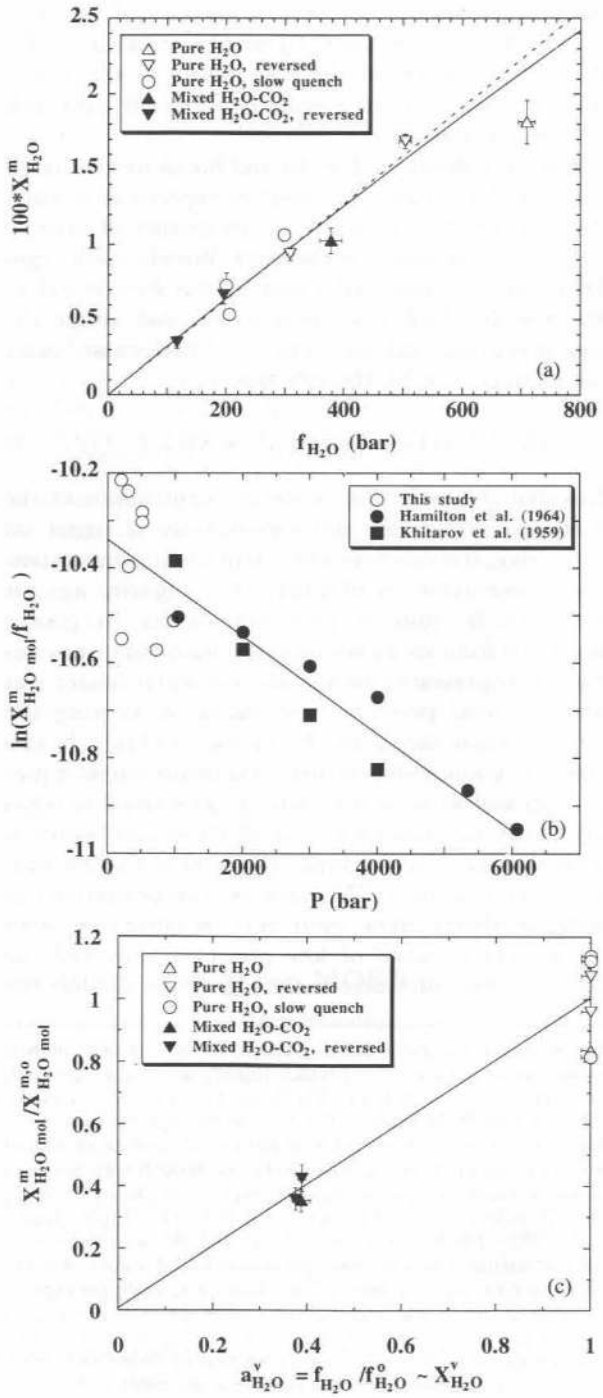

Fig. 5. (a) Linear relationship between molecular H_2O, determined from the 5200 cm^{-1} absorbance, and f_{H_2O} indicating Henrian behavior over pressure range investigated. Error bars are 1σ errors from Table 1; symbols with no error bars have errors smaller than the size of the symbol. Dotted line is linear fit based on $P < 510$ bar data ($X^m_{H_2O,mol} = (3{\cdot}2 \pm 0{\cdot}1) \times 10^{-5}$ f_{H_2O}, $R^2 = 0{\cdot}95$); continuous line is calculated from equation (2) using $a^m_{H_2O}$ (1 bar, 1200°C) = $(3{\cdot}28 \pm 0{\cdot}06) \times 10^{-5}$ and $V^{o,m}_{H_2O}$ of 12 ± 1 cm^3/mol. (b) ln $(X^m_{H_2O,mol}/f_{H_2O})$ vs P for basaltic glasses from this study, Khitarov *et al.* (1959) and Hamilton *et al.* (1964). Water activities in the higher-pressure experiments for which speciation measurements were not available were calculated assuming that the dependence of molecular water content on total water content can be described by the fit to the albitic glass speciation data. The slope of the line is $-V^{o,m}_{H_2O}/RT$ and gives a $V^{o,m}_{H_2O}$ of 12 ± 1 cm^3/mol. (c) Plot of $X^m_{H_2O,mol}/X^{m,o}_{H_2O,mol}$ vs $f_{H_2O}/f^o_{H_2O}$ showing that the ratio of the amount of molecular water dissolved in melt in equilibrium with mixed H_2O–CO_2 vapor phase to that dissolved in melt in equilibrium with a pure H_2O vapor phase calculated using our fit to equation (2) is equal to the ratio of the water fugacities in the mixed and pure vapors.

Fig. 4, where the solubility of water as a function of $P_{Total} = P_{H_2O}$ calculated using these parameters is compared with the data. Moreover, the extrapolated 1-atm solubility of water in basalt at 1200°C using these values is 0·11 wt %, in good agreement with values of 0·10–0·11 wt % based on experimental determinations of the water contents of vapor-saturated tholeiitic melt at 1 atm [(1) H_2–H_2O gas mixture, $X^v_{H_2O} = 0{\cdot}98$, total $H_2O = 0{\cdot}095$ wt %; (2) H_2–CO_2 mixture, $X^v_{H_2O} = 0{\cdot}05$, total $H_2O = 0{\cdot}026$ wt % (Baker & Grove, 1985; M. Baker, personal communication, 1993]. Calculated water solubilities using these parameters are listed in Table 5 (below) at various $P_{total} = P_{H_2O}$.

The assumption of constant $V^{o,m}_{H_2O}$ can be evaluated by plotting ln $(X^m_{H_2O,mol}/f_{H_2O})$ vs P (Fig. 5b), in which the slope of an isotherm is $-V^{o,m}_{H_2O}/RT$, again making the Henrian approximation that $a^m_{H_2O} \propto X^m_{H_2O,mol}$. It should be emphasized that $X^m_{H_2O,mol}$ values for the higher-pressure experiments are calculated from the total water contents using the extrapolation of the regular solution fit to the speciation data shown in Fig. 3b. The results are well described by a single straight line, corresponding to a constant $V^{o,m}_{H_2O}$ of 12 ± 1 cm^3/mol, although the scatter in our low-pressure data is too great to determine if there is a decrease in slope and thus in the partial molar volume of water at low pressures as has been proposed for rhyolitic melts by Silver *et al.* (1990). However, like the near-zero value for rhyolitic liquid (Silver *et al.*, 1990), our value for $V^{o,m}_{H_2O}$ in MORB liquid is lower than those for other silicate liquid compositions (17–25 cm^3/mol; Table 4).

In Fig. 5c we have plotted the ratio of the concentration of molecular water in the sample to its concentration in melt saturated with pure water vapor [this ratio is equal to the activity of water in the melt given the Henrian approximation if the standard state at each pressure and temperature is the water-saturated melt under the same conditions; this is equivalent to the standard state adopted by Burnham & Davis (1971)] versus ratio of the fugacity of water in each experiment to the fugacity of pure water under the same conditions (this ratio is equal to the activity of water in the vapor and approximately equal to the mole fraction of water in the vapor). The 1:1 relationship shown in Fig. 5c is an alternative way to demonstrate the validity of the Henrian approximation we have adopted and emphasizes that the effect of CO_2 in the vapor is simply one of dilution; i.e. the amount of molecular water that dissolves in the melt is lowered by the same factor by which the fugacity of water is lowered owing to the dilution of the vapor with CO_2 or any other vapor species.

CO_2 solubility in basaltic melts in equilibrium with mixed H_2O–CO_2 vapor

Nine successful experiments with a mixed H_2O–CO_2 vapor phase ($X^v_{CO_2} = 0{\cdot}42$–$0{\cdot}97$) were conducted in the rapid-quench IHPV at 1200°C at total pressure between 210 and 980 bar. Experimental conditions and dissolved carbonate and water concentrations are reported in Table 1. As discussed above, three experiments (Nos 18M, 20M and 21M) in which oxalic acid dihydrate was used to produce a mixed H_2O–CO_2 vapor phase have well-constrained H_2O and CO_2 fugacities based on manometric analysis of the quenched vapor or mass balance calculations. The vapor-phase composition for the other mixed vapor experiments could not be determined by mass

Table 4: Estimates of the partial molar volume of H_2O in silicate liquids

Composition	$V^{o,m}_{H_2O}$ (cm^3/mol)	P range (kbar)	T range (°C)	Reference
$NaAlSi_3O_8$	17–22	3–8	1000	Burnham & Davis (1971)
$NaAlSi_3O_8$	~22[a]	1–8	1000	Silver *et al.* (1990)
$KAlSi_3O_8$	~25	1–7	900–1340	Silver *et al.* (1990)
Ca–Al-silicate	~16	1–5	1180	Silver *et al.* (1990)
$CaMgSi_2O_6$	~17	20	1240	Hodges (1974)
Basalt	~12	0·18–8	1100–1200	This study and data from Khitarov *et al.* (1959) and Hamilton *et al.* (1964)
Rhyolite	~0	<1·5	850	Silver *et al.* (1990)

Modified from Lange & Carmichael (1990). [a]$V^{o,m}_{H_2O}$ may be much lower at low water contents as inferred by Silver & Stolper (1989).

Table 5: Model water speciation and water and carbon dioxide solubility in basaltic melt at 1200°C

P (bar)	f_{H_2O}[a] (bar)	$X_{H_2O,\,mol}$[b]	X_{OH}[c]	X_B[d]	H_2O (mol)[e] (wt%)	OH[f] (wt%)	H_2O, total[g] (wt%)	f_{CO_2}[a] (bar)	CO_2[h] (p.p.m.)
1	1	0·000	0·005	0·002	0·00	0·11	0·11	1	0·5
5	5	0·000	0·010	0·005	0·01	0·24	0·25	5	2
10	10	0·000	0·013	0·007	0·02	0·33	0·35	10	5
25	25	0·001	0·019	0·010	0·04	0·48	0·52	25	11
50	50	0·002	0·026	0·015	0·08	0·65	0·73	51	23
100	100	0·003	0·034	0·020	0·16	0·86	1·02	102	46
200	199	0·006	0·044	0·028	0·32	1·10	1·42	209	92
300	298	0·010	0·050	0·035	0·48	1·25	1·73	320	138
400	397	0·013	0·054	0·040	0·63	1·37	2·00	436	185
500	496	0·016	0·058	0·044	0·78	1·46	2·24	557	232
600	595	0·018	0·061	0·049	0·93	1·53	2·46	683	279
700	694	0·021	0·063	0·053	1·08	1·59	2·66	815	326
800	794	0·024	0·065	0·056	1·22	1·64	2·86	952	374
900	893	0·027	0·066	0·060	1·36	1·68	3·04	1100	422
1000	993	0·030	0·068	0·063	1·50	1·72	3·22	1240	471
2000	2032	0·055	0·075	0·092	2·83	1·93	4·76	3130	979
3000	3190	0·078	0·076	0·116	4·08	2·00	6·08	5920	1534
4000	4526	0·100	0·076	0·138	5·31	2·01	7·32	10000	2142
5000	6092	0·122	0·074	0·160	6·56	1·99	8·55	15850	2810

[a]Fugacity of pure water and carbon dioxide were calculated using a modified Redlich–Kwong equation of state (Holloway, 1977) assuming $P_{H_2O} = P_{Total}$ or $P_{CO_2} = P_{Total}$. [b]Mole fractions of molecular water in the melt were calculated using a Henrian model for the activity of water in the melt [Equation (2)] and a $V^{o,m}_{H_2O}$ of 12 cm^3/mol. [c]Mole fractions of hydroxyl groups were calculated using a regular solution model {Silver & Stolper, 1989); using $-\ln\left[\frac{(X^m_{OH})^2}{(X^m_{H_2O,mol})(1-X^m_{H_2O,mol})}\right] = A' + B'X^m_{OH} + C'X^m_{H_2O,\,mol}$, where $A' = 0{\cdot}403$, $B' = 15{\cdot}333$ and $C' = 10{\cdot}894$, and molecular weight for basalt of 36·594}.

[d]$X_B = X^m_{H_2O,\,mol} + X^m_{OH}/2$.

[e]wt %H_2O_{mol} = (1801·5X_B + 18·579 wt%$H_2O_{Tot}X^m_{H_2O_{mol}}$)/36·594.

[f]wt %OH = wt %H_2O_{Tot} − wt %H_2O_{mol}.

[g]wt %H_2O_{Tot} = 1801·5X_B/(36·594 − 18·579X_B).

[h]Mole fraction carbon dioxide in the melt calculated using equation (4) with a $V^{o,m}_{H_2O}$ of 23 cm^3/mol. Concentration of CO_2 (p.p.m.) calculated from 10^4 [4400$X^m_{CO_2}$/(36·594 − 44$X^m_{CO_2}$)].

balance because these experiments were conducted using pure Ar gas as the pressurizing medium, resulting in significant and variable amounts of H_2 loss from the capsule during the runs. Vapor-phase compositions for these runs were calculated indirectly via the following procedure. First, the water fugacity was determined from the measured concentration of molecular water in the quenched glass and the relation between water fugacity, total pressure and the mole fraction of molecular water in the melt [equation (2)]. As there is a unique correspondence between water fugacity and vapor composition at a given pressure and total pressure assuming the vapor is composed only of H_2O and CO_2, we were then able to determine the mole fractions of H_2O and CO_2 (and the fugacity of CO_2 in the vapor) at

the run conditions. The $X^{v}_{H_2O}$ values calculated in this way are 0·39 and 0·45 for runs Nos 20M and 21M versus manometrically determined values of 0·39 and 0·40. Based on this comparison, we estimate that the $X^{v}_{H_2O}$ values determined by this procedure are accurate to ~15%.

Concentrations of dissolved CO_2 in the experimental glasses range from 63 to 315 p.p.m. CO_2 and are proportional to the f_{CO_2} in the coexisting vapor (Fig. 6a). Carbonate is the only form of dissolved carbon detectable by infrared spectroscopy in these glasses, consistent with previous results on natural and synthetic basaltic glasses (Fine & Stolper, 1986; Stolper & Holloway, 1988; Dixon *et al.*, 1988; Dixon *et al.*, 1991). Also plotted are data from two glasses quenched from melts equilibrated with pure CO_2 vapor [TT152-2 and -5 from Stolper & Holloway (1988)] and data from Pawley *et al.* (1992) for glasses quenched from melts equilibrated with CO–CO_2 vapor. CO_2 concentrations in samples TT152-2 and -5 were reanalyzed for this study, so that all data were obtained using a consistent background-subtraction scheme, and are ~10% higher than the values reported by Stolper & Holloway (1988). The highest pressure run of Stolper & Holloway (1988) was not included in this data set because the run failed after an hour and could have anomalously low CO_2 concentrations (Stolper & Holloway, 1988). The data of Pawley *et al.* (1992) are systematically ~20% higher than ours at the same f_{CO_2}, but overlap with ours at the 1σ level (±15%). The CO_2 concentrations in basalt in equilibrium with a mixed H_2O–CO_2 vapor phase measured by Kadik *et al.* (1972) and Shilobreyeva & Kadik (1989) range from 2 to 20 times higher than those from this and other recent studies (Stolper & Holloway, 1988; Mattey, 1991; Pawley *et al.*, 1992; Trull *et al.*, 1992) and are not shown.

CO_2 concentrations of runs No. 33B (62±6 p.p.m., held at a total pressure of 503 bar for 2 h with f_{CO_2} = 207 bar) and No. 20M (72±7 p.p.m.,

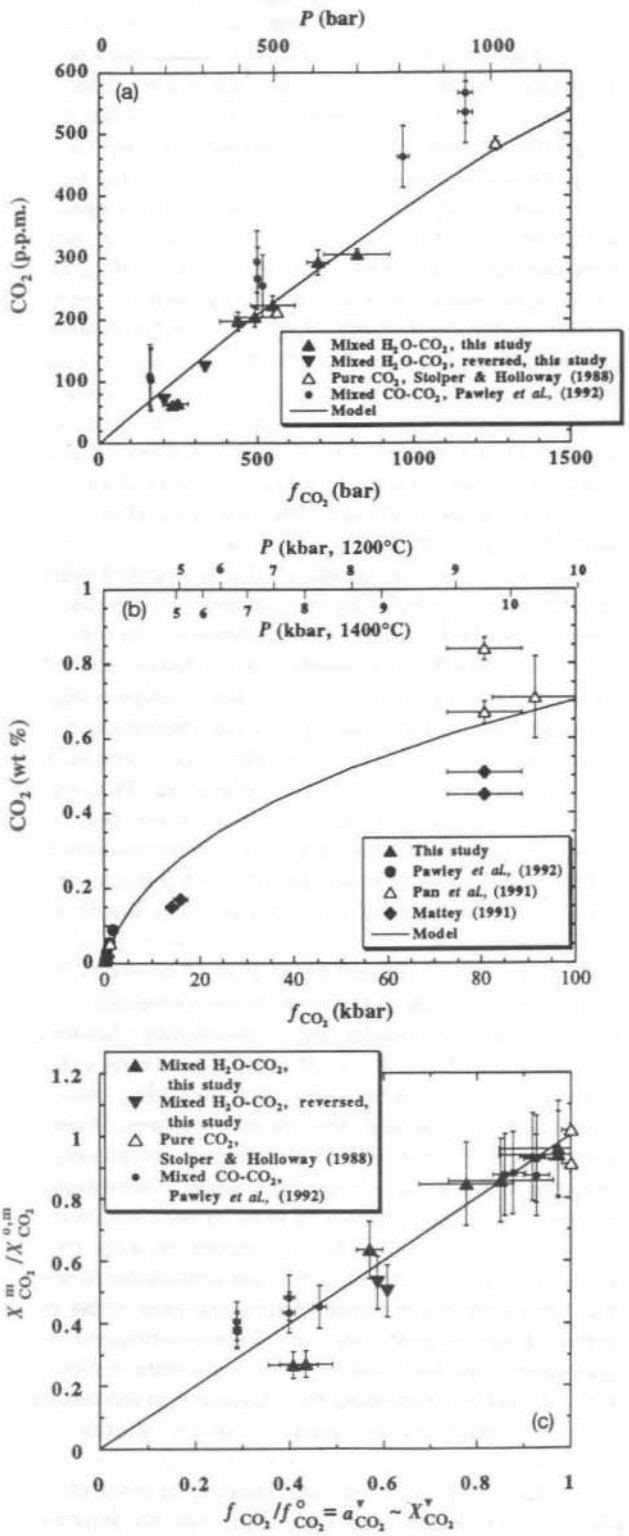

Fig. 6. (a) Concentration of CO_2 (p.p.m.) plotted against f_{CO_2} in basaltic glasses from this study and from Pawley *et al.* (1992), where melts were equilibrated with a mixed CO–CO_2 vapor phase. CO_2 fugacities calculated using MRK equations of state for H_2O–CO_2 mixtures (Holloway, 1977) and CO–CO_2 mixtures (Holloway, 1987). Curve calculated using equation (4) and shows that the solubility of carbon dioxide is a simple function of f_{CO_2} regardless of the composition of the vapor. The data of Pawley *et al.* (1992) are ~20% higher than ours. Errors for our data are 1σ from Table 1 and for Pawley *et al.* data are ±50 p.p.m. (b) Concentration of CO_2 (wt %) plotted against f_{CO_2} comparing the fit to our low-pressure data with results of higher-pressure experiments. (c) $X^{m}_{CO_2}/X^{o,m}_{CO_2}$ vs $f_{CO_2}/f^{o}_{CO_2}$ showing that the ratio of the amount of carbon dioxide dissolved in melt in equilibrium with mixed H_2O–CO_2 or CO–CO_2 vapor phases with respect to that dissolved in melt in equilibrium with a pure CO_2 vapor phase is equal to the activity of CO_2 in the vapor. Because the data of Pawley *et al.* (1992) are systematically higher than ours by ~20%, $X^{o,m}_{CO_2}$ values were calculated using equation (6) and best-fit values for $a^{o,m}_{CO_2}$ of $3{\cdot}8\times10^{-7}$ for data from this study and $5{\cdot}3\times10^{-7}$ for data from Pawley *et al.* (1992).

held at a total pressure of 424 bar for 3 h followed by 310 bar for 3 h with a final $f_{CO_2} = 201$ bar) agree within error, indicating that equilibrium was reached on the time scales of the experiments. Moreover, the agreement of the CO_2 concentrations in the No. 33B–No. 20M experiment pair (different total pressures, but similar f_{CO_2}), and also in the pair No. 35B (mixed H_2O–CO_2 vapor, $f_{CO_2} = 531$ bar) and TT152-5 from Stolper & Holloway (1988; pure CO_2 vapor, $f_{CO_2} = 560$ bar) shows that the solubility of carbon dioxide as carbonate at these low pressures is a simple function of f_{CO_2}, regardless of total pressure or the composition of the vapor. This is also demonstrated by the similarity of our results on melts saturated with pure CO_2 and H_2O–CO_2 vapor to those of Pawley *et al.* (1992) on melts saturated with CO–CO_2 vapor (Fig. 6a).

The solubility of carbon dioxide in basaltic melts can be described by the following reaction (see Stolper & Holloway, 1988):

$$CO_2 \text{ (vapor)} + O^{2-} \text{ (melt)} = CO_3^{2-} \text{ (melt)}. \quad (4)$$

The equilibrium constant for the reaction at P and T is

$$K(P)T = \frac{a^{m}_{CO_3^{2-}}(P, T)}{a^{m}_{O^{2-}}(P, T) f_{CO_2}(P, T)} \quad (5)$$

where $f_{CO_2}(P,T)$ is the fugacity of carbon dioxide in the vapor coexisting with the melt and the activities of carbonate and oxygen in the melt are relative to standard states defined by the pure melt species at the temperature and pressure of interest, such that $a^{m}_{O^{2-}}(P,T) = 1$ for CO_2-free melt at P and T and $a^{m}_{CO_3^{2-}}(P,T) = 1$ for a hypothetical melt consisting only of carbonate groups. Assuming the melt can be treated as an ideal mixture of CO_3^{2-} groups and O^{2-} ions (Fine & Stolper, 1985; Stolper *et al.*, 1987), then the activities in equation (5) can be replaced by mole fractions of each species (see footnote to Table 1). Because $X^{m}_{CO_3^{2-}}$ is so small, the $X^{m}_{O^{-2}}$ terms at P and P_0 effectively cancel, resulting in the following expression for the pressure dependence of activity of dissolved carbonate at constant temperature (T_0):

$$X^{m}_{CO_3^{2-}}(P, T) =$$

$$X^{m}_{CO_3^{2-}}(P_0, T_0) \frac{f_{CO_2}(P, T_0)}{f_{CO_2}(P_0, T_0)} \exp\left\{\frac{-\Delta V_r^{o,m}(P - P_0)}{RT_0}\right\} \quad (6)$$

where $\Delta V_r^{o,m} = (V^{o,m}_{CO_3^{2-}}) - (V^{o,m}_{O^{2-}})$ and $V^{o,m}_{O^{2-}}$ and $V^{o,m}_{CO_3^{2-}}$) are the molar volumes of the melt species in their standard states and have been taken to be independent of P and T in deriving equation (6).

Taking $P_0 = 1$ bar, $T_0 = 1200°C$, and $\Delta V_r^{o,m} = 23$ cm^3/mol (Pan *et al.*, 1991), the best-fit value for $X^{m}_{CO_3^{2-}}$ (1 bar, 1200°C) is $(3{\cdot}8 \pm 0{\cdot}1) \times 10^{-7}$ based on our data [or $(4{\cdot}8 \pm 0{\cdot}2) \times 10^{-7}$ based on our data plus the data of Pawley *et al.* (1992) for CO–CO_2-saturated melts]. The correspondence between the curve calculated using these parameters and our data (Fig. 6a) demonstrates the suitability of the Henrian approximation for the carbonate species in basaltic melt under these conditions. The 1-atm solubility of carbon dioxide in basalt at 1200°C using these values is calculated to be 0·5 p.p.m. by weight. Calculated CO_2 solubilities over a range of pressures are listed in Table 5. A useful, but less precise [because of the volume term in equation (4) and the varying fugacity coefficient for CO_2 even under these conditions] rule of thumb for CO_2 solubility at total pressures less than ~800 bar is that the solubility increases ~47 p.p.m. for every pressure increase of 100 bar (equivalent to 47 p.p.m. per km water depth). When extended to higher pressures (Fig. 6b), our model parameters for CO_2 solubility give values intermediate between the results of Pan *et al.* (1991) and Mattey (1991).

The best-fit value for $a^{m}_{CO_3^{2-}}$ (1 bar, 1200°C) based on our data is ~30% higher than the value given by Stolper & Holloway (1988). Several factors contribute to the higher solubility estimate, including more data, improvements in the background-subtraction procedure (leading to an increase in concentration of ~10% for the two reanalyzed samples), and omission of Stolper & Holloway's highest pressure run. This revision does not, however, imply that the CO_2 concentrations data reported by Dixon *et al.* (1988) are systematically low by 20% as recently suggested by Blank *et al.* (1993*b*).

The assumed value of $\Delta V_r^{o,m}$ from Pan *et al.* (1991) is sufficiently high that the pressure-dependent term in equation (4) results in a noticeable downward curvature of the calculated solubility vs f_{CO_2} curve even at pressures as low as 1000 bar (Fig. 6a); the effect of this term is dramatic at pressures of several thousand bars (Fig. 6b). This effect is, however, still too small for us to detect differences between dissolved carbonate contents of runs in which variations in f_{CO_2} were produced by variations in vapor composition at constant total pressure and those in which the variations were produced by varying total pressure. Consequently, all our vapor-saturated CO_2 concentrations fall within error on a single curve in Fig. 6a, again validating the Henrian approximation for CO_2 solution in basaltic melts under these conditions.

As discussed for molecular water, the validity of the Henrian model for CO_2 solution in basaltic melts

in equilibrium with H_2O–CO_2 vapor can also be illustrated on a plot of $(X^{m}_{CO_2}/X^{o,m}_{CO_2})$ vs $(f_{CO_2}/f^{o}_{CO_2})$ (Fig. 6c). All data shown in Fig. 6c, including those for CO–CO_2-saturated basaltic melts (Pawley *et al.*, 1992), correspond reasonably well to the 1:1 line. Most importantly, the Henrian model for the activity of carbonate in the melt is valid even for melts coexisting with CO_2-rich vapor, where a significant enhancement of CO_2 concentration relative to the 1:1 line was expected based on studies of CO_2 concentrations in melts saturated with CO_2–H_2O vapors at significantly higher pressure (Eggler, 1973; Holloway & Lewis, 1974; Kadik & Eggler, 1975; Mysen *et al.*, 1975, 1976; Brey & Green, 1976; Mysen, 1976; Eggler & Rosenhauer, 1978; Holloway, 1981). The difference between our results and previous studies that reported non–Henrian behavior of CO_2 (i.e. an enhancement of up to 50% in the amount of CO_2 that dissolves in silicate melts when $X^{v}_{CO_2}$ decreases from 1·0 to 0·8) could be that our experiments were conducted at significantly lower total pressures, where the amounts of dissolved water are much lower. In other words, the small amounts of water dissolved in our experiments (<3 wt %) may be insufficient to produce a detectable effect on CO_2 solution. We also note that similar Henrian behavior was observed at low pressures for rhyolitic melts, in which carbon dioxide is dissolved nearly entirely as CO_2 molecules (Blank *et al.*, 1993*a*). Further work will be needed to substantiate the higher-pressure effect and to study the transition between Henrian behavior we have observed and the more complex behavior observed at higher pressures.

It is significant that Henry's law describes so well the solution of CO_2 in basaltic melts, regardless of whether the coexisting vapor is pure CO_2 or diluted with H_2O or CO. It considerably simplifies calculations of the degassing of basaltic melts during ascent and eruption, as the thermodynamics of CO_2 and H_2O solution are so simple. In particular, thermodynamic properties determined in the end-member systems can be accurately applied to calculating solubilities in the mixed volatile systems, as these two components (and CO) do not appear to influence each other's activity coefficients in melt. This is not to say that the presence of H_2O in the vapor does not influence the amount of CO_2 that will dissolve in the coexisting melt: the decrease in the activity of CO_2 in the vapor owing to its dilution with H_2O (or CO or other gaseous species) will produce a proportionate decrease in the amount of CO_2 dissolved in the melt. Likewise, the amount of molecular H_2O dissolved in the melt will decrease relative to that in a melt saturated with pure H_2O by an amount proportional to the decreased activity of H_2O in the vapor, owing to its dilution with CO_2 or other gaseous species.

SUMMARY

A series of experiments at 1200°C and pressures from 200 to 980 bar have been performed to determine the solubilities of H_2O and CO_2 and the nature of their mixing behavior in basaltic liquid at conditions relevant to seafloor eruption. Our major results are as follows:

(1) The IR spectroscopic technique has been calibrated in the near-IR region for basaltic glass to determine concentrations of hydrous species. Molar absorptivities for the 4500 cm^{-1} band for hydroxyl groups and for the 5200 and 1630 cm^{-1} bands for molecular water are $0{\cdot}67 \pm 0{\cdot}03$, $0{\cdot}62 \pm 0{\cdot}07$, and 25 ± 3 l/mol-cm, respectively. Molar absorptivities determined in several laboratories on a range of glass compositions correlate positively and linearly with the concentration of tetrahedral cations $(Si^{4+} + Al^{3+})$.

(2) The trends in water speciation in quenched MORB glasses are indistinguishable from those in albitic glasses quenched from 1400°C and can be modeled using a regular ternary solution model with the coefficients for albitic glasses (Silver & Stolper, 1989).

(3) Activities of both molecular water and carbonate in basaltic melt follow Henry's law at the low pressures of our experiments. In contrast to previous studies at higher pressures that reported non-Henrian behavior of CO_2 (i.e. an enhancement of up to 50% in the amount of CO_2 that dissolves in silicate melts when $X^{v}_{CO_2}$ decreases from 1·0 to 0·8), water did not enhance the solution of CO_2 as carbonate in our experiments. It is significant that Henry's law describes so well the solution of CO_2 in basaltic melts, regardless of whether the coexisting vapor is pure CO_2 or diluted with H_2O or CO, because it means that the thermodynamic properties determined in the end-member systems can be accurately used in calculating saturation concentrations of H_2O and CO_2 in mixed volatile systems.

(4) Experimental results for water solubility in MORB at pressures from 200 to 980 bar are consistent with those of previous studies at higher pressures. A best fit to our data and existing higher-pressure water solubility data gives estimates for $X^{o,m}_{H_2O}$ of 12 ± 1 cm^3/mol and for the $a^{m}_{H_2O}$ (1 bar, 1200°C) of $(3{\cdot}28 \pm 0{\cdot}06) \times 10^{-5}$ (equivalent to a 1 bar water solubility of 0·11 wt %).

(5) A best fit through our experimental results for CO_2 solubility in MORB at low pressures using a $\Delta V^{o,m}_{r}$ of 23 cm^3/mol (Pan *et al.*, 1991) yields an

$a^{o,m}_{CO_3^{2-}}$ (1 bar, 1200°C) of $3{\cdot}8 \times 10^{-7}$ (equivalent to a 1-bar CO_2 solubility of 0·5 p.p.m.). Our estimate of CO_2 solubility is ~20% higher than that reported by Stolper & Holloway (1988).

ACKNOWLEDGEMENTS

This work was supported by NSF Grants NSF EAR-8811406, EAR8617128 and OCE88-20131. We thank Ian Carmichael for FeO analyses on the glasses, Phil Ihinger for providing manometric analyses, and Mike Baker, John Beckett, David Bell, Jen Blank, Rick Hervig, David Joyce, Jim Kubicki, Greg Miller, Gordon Moore, Sally Newman, Vivian Pan, Alison Pawley, George Rossman, Tom Stanton and Sieger Van der Laan for assistance and advice. This paper is Caltech Division of Geological and Planetary Sciences Contribution 5632.

REFERENCES

Acocella, J., Tomozawa, M. & Watson, E. B., 1984. The nature of dissolved water in sodium silicate glasses and its effect on various properties. *Journal of Non-Crystalline Solids* **65,** 355–372.

Armstrong, J. T., 1982. New ZAF and a-factor correction procedures for the quantitative analysis of individual microparticles. In: K. F. J. Heinrich (ed.) *Microbeam Analysis*—1982. San Francisco, CA: San Francisco Press, pp. 175–180.

Armstrong, J. T., 1988. Quantitative analysis of silicate and oxide materials: comparison of Monte Carlo, ZAF, and $\phi(\rho z)$ procedures. In: D. E. Newbury (ed.) *Microbeam Analyses*—1988. San Francisco, CA: San Francisco Press, pp. 239–246.

Baker, M. B. & Grove, T. L., 1985. Kinetic controls on pyroxene nucleation and metastable liquid lines of descent in a basaltic andesite. *American Mineralogist* **70,** 279–287.

Bartholomew, R. F. & Schreurs, J. W. H., 1980. Wide-line NMR study of protons in hydrosilicate glasses of different water content. *Journal of Non-Crystalline Solids* **38–39,** 679–684.

Bartholomew, R. F., Butler, B. L., Hoover, H. L. & Wu, C. K., 1980. Infrared spectra of a water-containing glass. *Journal of the American Ceramic Society* **63,** 481–485.

Bell, P. M., Mao, H. K. & Weeks, R. A., 1976. Optical spectra and electron paramagnetic resonance of lunar and synthetic glasses: a study of the effects of controlled atmosphere, composition, and temperature. *Proceedings of the 7th Lunar Science Conference. Geochimica et Cosmochimica Acta Supplement* 2543–2559.

Bevington, P. R., 1969. *Data Reduction and Error Analysis for the Physical Sciences.* New York: McGraw–Hill, p. 336.

Bigeleisen, J., Perlman, M. L. & Prosser, H. C., 1952. Conversion of hydrogenic materials to hydrogen for isotopic analysis. *Analytical Chemistry* **24,** 1356–1357.

Blank, J. G., Stolper, E. M. & Carroll, M. R., 1993*a*. Solubilities of carbon dioxide and water in rhyolitic melt at 850°C and 750 bars. *Earth and Planetary Science Letters* **119,** 27–36.

Blank, J. G., Delaney, J. R. & Des Marais, D. J., 1993*b*. The concentration and isotopic composition of carbon in basaltic glasses from the Juan de Fuca Ridge. *Geochimica et Cosmochimica Acta* **57,** 875–887.

Bottinga, Y. & Javoy, M., 1990. MORB degassing: bubble growth and ascent. *Chemical Geology* **81,** 255–270.

Brey, G. P. & Green, D. H., 1975. The role of CO_2 in the genesis of olivine melilitite. *Contributions to Mineralogy and Petrology* **49,** 93–103.

Brey, G. P. & Green, D. H., 1976. Solubility of CO_2 in olivine melilitite at high pressures and role of CO_2 in the Earth's upper mantle. *Contributions to Mineralogy and Petrology* **55,** 217–230.

Buerger, M. J., 1948. The structural nature of the mineralizer action of fluorine and hydroxyl. *American Mineralogist* **33,** 744–746.

Burnham, C. W., 1975. Water and magmas: a mixing model. *Geochimica et Cosmochimica Acta* **39,** 1077–1084.

Burnham, C. W. & Davis, N. F., 1971. The role of H_2O in silicate melts: I. *P–V–T* relations in the system $NaAlSi_3O_8$–H_2O to 1 kilobar and 1000°C. *American Journal of Science* **270,** 54–79.

Burnham, C. W. & Jahns, R. H., 1962. A method for determining the solubility of water in silicate melts. *American Journal of Science* **260,** 721–745.

Carmichael, I. S. E. & Ghiorso, M. S., 1986. Oxidation–reduction relations in basic magma: a case for homogeneous equilibria. *Earth and Planetary Science Letters* **78,** 200–210.

Christie, D. M., Carmichael, I. S. E. & Langmuir, C. H., 1986. Oxidation states of mid-ocean ridge basalt glasses. *Earth and Planetary Science Letters* **79,** 397–411.

Clague, D. A., Weber, W. S. & Dixon, J. E., 1991. Picritic glasses from Hawaii. *Nature* **353,** 553–556.

Delaney, J. R., Muenow, D. W. & Graham, D. G., 1978. Abundance and distribution of water, carbon and sulfur in the glassy rims of submarine pillow basalts. *Geochimica et Cosmochimica Acta* **42,** 581–594.

Des Marais, D. J., 1985. Carbon exchange between the mantle and the crust, and its effect upon the atmosphere: today compared to Archean time. *Geophysical Monograph, American Geophysical Union* **32,** 602–611.

Dingwell, D. B. & Webb, S. L., 1990. Relaxation in silicate melts. *European Journal of Mineralogy* **2,** 427–449.

Dixon, J. E. & Stolper, E. M., 1995. An experimental study of water and carbon dioxide solubilities in mid-ocean ridge basaltic liquids. Part II: Applications to degassing. *Journal of Petrology* **36,** 1633–1646.

Dixon, J. E., Stolper, E. & Delaney, J. R., 1988. Infrared spectroscopic measurements of CO_2 and H_2O glasses in the Juan de Fuca Ridge basaltic glasses. *Earth and Planetary Science Letters* **90,** 87–104.

Dixon, J. E., Clague, D. A. & Stolper, E. M., 1991. Degassing history of water, sulfur, and carbon in submarine lavas from Kilauea volcano, Hawaii. *Journal of Geology* **99,** 371–394.

Dodd, D. M. & Fraser, D. B., 1966. Optical determinations of OH in fused silica. *Journal of Applied Physics* **37,** 3911.

Eckert, H., Yesinowski, J. P. & Stolper, E. M., 1989. Quantitative NMR studies of water in silicate glasses. *Solid State Ionics* **32–33,** 298–313.

Eggler, D. H., 1973. Role of CO_2 in melting processes in the mantle. *Carnegie Institution of Washington, Yearbook* **72,** 457–467.

Eggler, D. H. & Rosenhauer, M., 1978. Carbon dioxide in silicate melts: II. Solubilities of CO_2 and H_2O in $CaMgSi_2O_6$ (diopside) liquids and vapors at pressures to 40 kb. *American Journal of Science* **278,** 64–94.

Eugster, H. P. & Skippen, G. B., 1967. Igneous and metamorphic reactions involving gas equilibria. In: P. H. Abelson (ed.) *Researches in Geochemistry* **2.** New York: John Wiley, pp. 492–520.

Fine, G. & Stolper, E., 1985. The speciation of carbon dioxide in sodium aluminosilicate glasses. *Contributions to Mineralogy and Petrology* **91,** 105–121.

Fine, G. & Stolper, E., 1986. Carbon dioxide in basaltic glasses: concentrations and speciation. *Earth and Planetary Science Letters* **76,** 263–278.

Gerlach, T. M., 1986. Exsolution of H_2O, CO_2, and S during eruptive episodes at Kilauea Volcano, Hawaii. *Journal of Geophysical Research* **91,** 12177–12185.

Gerlach, T. M., 1989. Degassing of carbon dioxide from basaltic magma at spreading centers: II. Mid-oceanic ridge basalts. *Journal of Volcanology and Geothermal Research* **39,** 221–232.

Goldman, D. S. & Berg, J. I., 1980. Spectral study of ferrous iron in Ca–Al–borosilicate glass at room and melt temperatures. *Journal of Non-Crystalline Solids* **38–39,** 183–188.

Gudmundsson, G. & Holloway, J. R., 1993. Activity–composition relationships in the system Fe–Pt at 1300 and 1400°C and at 1 atm and 20 kb. *American Mineralogist* **78,** 178–186.

Hamilton, D. L., Burnham, C. W. & Osborn, E. F., 1964. The solubility of water and effects of oxygen fugacity and water content on crystallization in mafic magmas. *Journal of Petrology* **5,** 21–39.

Hodges, F. W., 1974. The solubility of H_2O in silicate melts. *Carnegie Institution of Washington, Yearbook* **73,** 251–255.

Holloway, J. R., 1971. Internally-heated pressure vessels. In: Ulmer, G. C. (ed.) *Research Techniques for High Pressure and High Temperature*. New York: Springer-Verlag, pp. 217–258.

Holloway, J. R., 1977. Fugacity and activity of molecular species in supercritical fluids. In: Fraser, D. (ed.) *Thermodynamics in Geology*. Boston, MA: D. Reidel, pp. 161–181.

Holloway, J. R., 1981. Volatile interactions in magmas. In: Newton, R. C., Navrotsky, A. & Wood, B. J. (eds) *Thermodynamics of Melts and Minerals*. New York: Springer-Verlag, pp. 273–293.

Holloway, J. R., 1987. Igneous fluids. In: Carmichael, I. S. E. & Eugster, H. P. (eds) *Thermodynamic Modeling of Geological Materials: Minerals, Fluids and Melts. Mineralogical Society of America, Reviews in Mineralogy* **17,** 211–233.

Holloway, J. R. & Lewis, C. F., 1974. CO_2 solubility in hydrous albite liquid at 5 kb. *EOS Transactions American Geophysical Union* **55,** 483.

Holloway, J. R. & Reese, R. L., 1974. The generation of N_2–CO_2–H_2O fluids for use in hydrothermal experimentation 1: Experimental method and equilibrium calculations in the C–O–H–N system. *American Mineralogist* **59,** 587–597.

Holloway, J. R., Burnham, C. W. & Millhollen, G. L., 1968. Generation of H_2O–CO_2 mixtures for use in hydrothermal experimentation. *Journal of Geophysical Research* **73,** 6598–6600.

Holloway, J. R., Dixon, J. E. & Pawley, A. R., 1992. An internally-heated, rapid-quench high-pressure vessel. *American Mineralogist* **77,** 643–646.

Huebner, J. S., 1971. Buffering techniques for hydrostatic systems at elevated pressures. In: Ulmer, G. C. & Barnes, H. L., Jr (eds) *Research Techniques for High Pressure and High Temperature*. New York: Springer-Verlag, pp. 123–177.

Ihinger, P. D., 1991. An experimental study of the interaction of water with granitic melt. Ph.D. Thesis, California Institute of Technology, Pasadena, 188 pp.

Jambon, A. & Zimmermann, J. L., 1987. Major volatiles from a North Atlantic MORB glass and calibration to He: a size fraction analysis. *Chemical Geology* **62,** 177–189.

Jambon, A., Weber, H. W. & Begemann, F., 1985. Helium and argon from an Atlantic MORB glass: concentration, distribution and isotopic composition. *Earth and Planetary Science Letters* **73,** 255–267.

Jambon, A., Weber, H. & Braun, O., 1986. Solubility of He, Ne, Ar, Kr and Xe in a basalt melt in the range 1250–1600°C. Geochemical implications. *Geochimica et Cosmochimica Acta* **50,** 401–408.

Jambon, A., Zhang, Y. & Stolper, E. M., 1992. Experimental dehydration of natural obsidian and estimation of D_{H_2O} at low water contents. *Geochimica et Cosmochimica Acta* **56,** 2931–2935.

JANAF, 1986. *JANAF Thermochemical Tables*, 3rd edn. *Journal of Physics and Chemistry Reference Data* **14,** Supplement 1.

Javoy, M., Pineau, F. & Allègre, C. J., 1982. Carbon geodynamical cycle. *Nature* **300,** 171–173.

Joyce, D. B. & Holloway, J. R., 1993. An experimental determination of the thermodynamic properties of H_2O–CO_2–NaCl fluids at high pressures and temperatures. *Geochimica et Cosmochimica Acta* **57,** 733–746.

Kadik, A. A. & Eggler, D. H., 1975. Melt–vapor relations on the join $NaAlSi_3O_8$–H_2O–CO_2. *Carnegie Institute of Washington, Yearbook* **74,** 479–484.

Kadik, A. A., Lebedev, Ye. B. & Khitarov, N. I., 1971. *Voda v silikatnykh rasplavov. (Water in Silicate Melts.)* Moscow: Nauka.

Kadik, A. A., Lukanin, O. A., Lebedev, Ye. B. & Korovughkina, E. Ye., 1972. Solubility of H_2O and CO_2 in granite and basalt melts at high pressures. *Geochemistry International* **9,** 1041–1051.

Khitarov, N. I., Lebedev, E. B., Rengarten, E. V. & Arsenieva, R. V., 1959. Comparative characteristics of the solubility of water in basaltic and granitic melts. *Geochemistry (Geokhimiya)* **5,** 479–492.

Kilinc, A., Carmichael, I. S. E., Rivers, M. L. & Sack, R. O., 1983. Ferric–ferrous ratio of natural silicate liquids equilibrated in air. *Contributions to Mineralogy and Petrology* **83,** 136–140.

Killingley, J. S. & Muenow, D. W., 1975. Volatiles from Hawaiian submarine basalts determined by dynamic high temperature mass spectrometry. *Geochimica et Cosmochimica Acta* **39,** 1467–1473.

Kohn, S. C., Dupree, R. & Smith, M. E., 1989. A multinuclear magnetic resonance study of the structure of hydrous albite glasses. *Geochimica et Cosmochimica Acta* **53,** 2925–2935.

Kohn, S. C., Dupree, R. & Golam Mortuza, M., 1992. The interaction between water and aluminosilicate magmas. *Chemical Geology* **96,** 399–409.

Kohn, S. C., Smith, M. E. & Dupree, R., 1994. Comment on 'A model for H_2O solubility mechanisms in albite melts from infrared spectroscopy and molecular orbital calculations' by D. Sykes and J. D. Kubicki. *Geochimica et Cosmochimica Acta* **58,** 1377–1380.

Lange, R. & Carmichael, I. S. E., 1989. Ferric–ferrous equilibria in Na_2O–FeO–Fe_2O_3–SiO_2 melts: effects of analytical techniques on derived partial molar volumes. *Geochimica et Cosmochimica Acta* **53,** 2195–2204.

Lange, R. & Carmichael, I. S. E., 1990. Thermodynamic properties of silicate liquids with emphasis on density, thermal expansion and compressibility. In: Nicholls, J. & Russell, J. K. (eds) *Modern Methods of Igneous Petrology: Understanding Magmatic Processes. Mineralogical Society of America, Reviews in Mineralogy* **24,** 25–64.

Love, G., Cox, M. G. & Scott, V. D., 1978. A versatile atomic number correction for electron-probe microanalysis. *Journal of Physics*, D **11,** 7–27.

Marty, B. & Jambon, A., 1987. C/^{3}He in volatile fluxes from the solid earth: implications for carbon geodynamics. *Earth and Planetary Science Letters* **83,** 16–26.

Mathez, E. A., 1984. Influence of degassing on oxidation states of basaltic magmas. *Nature* **310,** 371–375.

Mattey, D., 1991. Carbon dioxide solubility and carbon isotope fractionation in basaltic melt. *Geochimica et Cosmochimica Acta* **55,** 3467–3473.

McMillan, P. F. & Holloway, J. R., 1987. Water solubility in aluminosilicate melts. *Contributions to Mineralogy and Petrology* **97,** 320–332.

McMillan, P. F., 1994. Water solubility and speciation models. In: Carroll, M. R. & Holloway, J. R. (eds) *Volatiles in Magmas. Mineralogical Society of America, Reviews in Mineralogy* **30,** 131–156.

McMillan, P. F. & Remmele, R. L., Jr, 1986. Hydroxyl sites in SiO_2 glass: a note on infrared and Raman spectra. *American Mineralogist* **71,** 772–778.

McMillan, P. F., Jakobsson, S., Holloway, J. R. & Silver, L. A., 1983. A note on the Raman spectra of water-bearing albite glasses. *Geochimica et Cosmochimica Acta* **47,** 1937–1943.

McMillan, P. F., Stanton, T. R., Poe, B. T. & Remmele, R. L., 1993. A Raman spectroscopic study of H/D isotopically substituted hydrous aluminosilicate glasses. *Physics and Chemistry of Minerals* **19,** 454–459.

Moore, J. G., 1965. Petrology of deep-sea basalt near Hawaii. *American Journal of Science* **263,** 40–52.

Moore, J. G., 1970. Water content of basalt erupted on the ocean floor. *Contributions to Mineralogy and Petrology* **28,** 272–279.

Moore, J. G., 1979. Vesicularity and CO_2 in mid-ocean ridge basalt. *Nature* **282,** 250–253.

Moore, J. G. & Schilling, J.-G., 1973. Vesicles, water, and sulfur in Reykjanes Ridge basalts. *Contributions to Mineralogy and Petrology* **41,** 105–118.

Moore, J. G., Batchelder, J. N. & Cunningham, C. G., 1977. CO_2-filled vesicles in mid-ocean basalt. *Journal of Volcanology and Geothermal Research* **2,** 309–327.

Mysen, B. O., 1976. The role of volatiles in silicate melts: solubility of carbon dioxide and water in feldspar, pyroxene, and feldspathoid melts to 30 kb and 1625°C. *American Journal of Science* **276,** 969–996.

Mysen, B. O., 1992. Peralkalinity, $Al \rightleftharpoons Si$ substitution, and solubility mechanisms of H_2O in aluminosilicate melts. *Journal of Petrology* **33,** 347–375.

Mysen, B. O. & Virgo, C., 1986. Volatiles in silicate melts at high pressure and temperature. 1. Interaction between OH groups and Si^{4+}, Al^{3+}, Ca^{2+}, Na^{+}, and H^{+}. *Chemical Geology* **57,** 303–331.

Mysen, B. O., Arculus, R. J. & Eggler, D. H., 1975. Solubility of carbon dioxide in melts of andesite, tholeiite, and olivine nephelinite composition to 30 kb pressure. *Contributions to Mineralogy and Petrology* **53,** 227–239.

Mysen, B. O., Eggler, D. H., Seitz, M. G. & Holloway, J. R., 1976. Carbon dioxide in silicate melts and crystals. Part I. Solubility measurements. *American Journal of Science* **276,** 455–479.

Nakamoto, K., 1978. *Infrared and Raman Spectra of Inorganic and Coordination Compounds*, 3rd edn. New York: John Wiley, 448 pp.

Newman, S., 1989. Water and carbon dioxide contents in basaltic glasses from the Mariana Trough. *EOS Transactions American Geophysical Union*, **70,** Fall Meeting Supplement, 1387.

Newman, S., 1990. Water and carbon dioxide contents of back arc basin basalts. *V. M. Goldschmidt Conference 1990, Program and Abstracts*, 69.

Newman, S., Stolper, E. M. & Epstein, S., 1986. Measurement of water in rhyolitic glasses: calibration of an infrared spectroscopic technique. *American Mineralogist* **71,** 1527–1541.

Newman, S., Epstein, S. & Stolper, E., 1988. Water, carbon dioxide, and hydrogen isotopes in glasses from the ca. 1340 A.D. eruption of the Mono Craters, California: constraints on degassing phenomena and initial volatile content. *Journal of Volcanology and Geothermal Research* **35,** 75–96.

Nilsson, K. & Peach, C., 1993. Sulfur speciation as a function of magmatic oxidation state: implications for sulfur concentrations in backarc and island arc magmas. *Geochimica et Cosmochimica Acta* **57,** 3807–3813.

Olbert, B. H. & Doremus, R. H., 1983. Infrared study of soda-lime glass during hydration and dehydration. *Journal of the American Ceramic Society* **66,** 163–166.

Pan, V., Holloway, J. R. & Hervig, R. L., 1991. The pressure and temperature dependence of carbon dioxide solubility in tholeiitic basalt melts. *Geochimica et Cosmochimica Acta* **55,** 1587–1595.

Pandya, N., Muenow, D. W. & Sharma, S. K., 1992*a*. The effect of bulk composition on the speciation of water in submarine volcanic glasses. *Geochimica et Cosmochimica Acta* **56,** 1875–1883.

Pandya, N., Sharma, S. K., Muenow, D. W. & Sherriff, B. L., 1992*b*. Hydration of alkali silicate glasses at ambient conditions. *EOS Transactions American Geophysical Union*, **73,** Spring Meeting Supplement, 361.

Pawley, A. R., Holloway, J. R. & McMillan, P., 1992. The effect of oxygen fugacity on the solubility of carbon–oxygen fluids in basaltic melt. *Earth and Planetary Science Letters* **110,** 213–225.

Pichavant, M., Holtz, F. & McMillan, P., 1992. Phase relations and compositional dependence of H_2O solubility in quartz–feldspar melts. *Chemical Geology* **96,** 303–319.

Reed, S. J. B., 1965. Characteristic fluorescence correction in electron-probe microanalysis. *British Journal of Applied Physics* **16,** 913–926.

Sato, M., 1978. Oxygen fugacity of basaltic magmas and the role of gas-forming elements. *Geophysical Research Letters* **5,** 447–449.

Scholze, H., 1959. Der Einbau des Wassers in Gläsern. *Glastechnische Berichte* **32,** 81–88, 142–145, 278–281.

Scholze, H., 1960. Zur Frage der Unterscheidung zwischen H_2O-Molekeln und OH-Gruppen in Gläsern und Mineralen. *Naturwissenschaften* **47,** 226–227.

Scholze, H., 1966. Gases and water in glass. *Glass Industry* **47,** 546–551, 622–628.

Sharma, S. K., 1979. Structure and solubility of carbon dioxide in silicate glasses of diopside and sodium melilite composition at high pressures from Raman spectroscopic data. *Carnegie Institution of Washington, Yearbook* **78,** 532–537.

Sharma, S. K., Hoering, T. C. & Yoder, H. S., 1979. Quenched melts of akermanite compositions with and without CO_2—characterization by Raman spectroscopy and gas chromatography. *Carnegie Institution of Washington, Yearbook* **78,** 537–542.

Shelby, J. E., Vitko, J., Jr, & Benner, R. E., 1982. Quantitative determination of the hydroxyl content of vitreous silica. *Journal of the American Ceramics Society* **65,** C59–C60.

Shilobreyeva, S. N. & Kadik, A. A., 1989. Solubility of CO_2 in magmatic melts at high temperatures and pressures. *Geokhimiya* **7,** 950–960.

Shilobreyeva, S. N., Kadik, A. A. & Lukanin, O. A., 1983. Outgassing of ocean-floor magma as a reflection of volatile conditions in the magma generation region. *Geokhimiya* **9,** 1257–1274.

Silver, L. A. & Stolper, E. M., 1989. Water in albitic glasses. *Journal of Petrology* **30,** 667–709.

Silver, L. A., Ihinger, P. D. & Stolper, E. M., 1990. The influence of bulk composition on the speciation of water in silicate glasses. *Contributions to Mineralogy and Petrology* **104,** 142–162.

Stolper, E., 1982*a*. Water in silicate glasses: an infrared spectroscopic study. *Contributions to Mineralogy and Petrology* **81,** 1–17.

Stolper, E., 1982*b*. The speciation of water in silicate melts. *Geochimica et Cosmochimica Acta* **46,** 2609–2620.

Stolper, E., 1989. Temperature dependence of the speciation of water in rhyolitic melts and glasses. *American Mineralogist* **74,** 1247–1257.

Stolper, E. M. & Holloway, J. R., 1988. Experimental determination of the solubility of carbon dioxide in molten basalt at low pressure. *Earth and Planetary Science Letters* **87,** 397–408.

Stolper, E., Fine, G., Johnson, T. & Newman, S., 1987. The solubility of carbon dioxide in albitic melt. *American Mineralogist* **72,** 1071–1085.

Sykes, D. & Kubicki, J. D., 1993. A model of H_2O solubility mechanisms in albite melts from infrared spectroscopy and molecular orbital calculations. *Geochimica et Cosmochimica Acta* **57,** 1039–1052.

Sykes, D. & Kubicki, J. D., 1994. Reply to the Comment by S. C. Kohn, M. E. Smith, and R. Dupree on 'A model for H_2O solubility mechanisms in albite melts from infrared spectroscopy and molecular orbital calculations'. *Geochimica et Cosmochimica Acta* **58,** 1381–1384.

Towozawa, M., Takata, M., Acocella, J., Watson, E. B. & Takamori, T., 1983. Thermal properties of $Na_2O_3 \cdot SiO_2$ glasses with high water content. *Journal of Non-Crystalline Solids* **56,** 343–348.

Trull, T., Pineau, F., Bottinga, Y. & Javoy, M., 1992. CO_2 bubble growth and $^{13}C/^{12}C$ isotopic fractionation in basaltic melt. *EOS Transactions American Geophysical Union,* **73,** Spring Meeting Supplement, 348.

Van der Laan, S. R. & Koster van Groos, A. F., 1991. Platinum-rich alloys in experimental petrology applied to high pressure research on hydrous iron-bearing systems. *American Mineralogist* **76,** 1920–1929.

Wallace, P. & Carmichael, I. S. E., 1992. Sulfur in basaltic magmas. *Geochimica et Cosmochimica Acta* **56,** 1863–1874.

Wilson, A. D., 1960. The micro-determination of ferrous iron in silicate minerals by a volumetric and a colormetric method. *Analyst* **85,** 823–827.

Wu, C.-K., 1980, Stable silicate glasses containing up to 10 weight percent water. *Journal of Non-Crystalline Solids* **41,** 381–398.

Zhang, Y. & Stolper, E. M., 1991. Water diffusion in a basaltic melt. *Nature* **351,** 306–309.

Zhang, Y. & Zindler, A., 1989. Noble gas constraints on the evolution of the Earth's atmosphere. *Journal of Geophysical Research* **94,** 13719–13737.

Zhang, Y. & Zindler, A., 1993. Distribution and evolution of carbon and nitrogen in Earth. *Earth and Planetary Science Letters* **117,** 331–345.

Zhang, Y., Stolper, E. M. & Wasserburg, G. J., 1991. Diffusion of water in rhyolitic glasses. *Geochimica et Cosmochimica Acta* **55,** 441–456.

RECEIVED JANUARY 15, 1994
REVISED TYPESCRIPT ACCEPTED JANUARY 10, 1995